

Cite this: *Chem. Sci.*, 2024, **15**, 11321

All publication charges for this article have been paid for by the Royal Society of Chemistry

Coordination of $\text{Al}(\text{C}_6\text{F}_5)_3$ vs. $\text{B}(\text{C}_6\text{F}_5)_3$ on group 6 end-on dinitrogen complexes: chemical and structural divergences†

Leon Escomel, ^a Frederico F. Martins, ^b Laure Vendier, ^a Anaïs Coffinet, ^a Nicolas Queyriaux, ^a Vera Krewald ^{*b} and Antoine Simonneau ^{*a}

The coordination of the Lewis superacid tris(pentafluorophenyl)alane (AlCF) to phosphine-supported, group 6 bis(dinitrogen) complexes $[\text{ML}_2(\text{N}_2)_2]$ is explored, with $\text{M} = \text{Cr}$, Mo or W and $\text{L} = \text{dppe}$ (1,2-bis(diphenylphosphino)ethane), depe (1,2-bis(diethylphosphino)ethane), dmpe (1,2-bis(dimethylphosphino)ethane) or $2 \times \text{PMe}_2\text{Ph}$. Akin to tris(pentafluorophenyl)borane (BCF), AlCF can form 1:1 adducts by coordination to one distal nitrogen of general formula $\text{trans-}[\text{ML}_2(\text{N}_2)\{(\mu-\eta^1:\eta^1-\text{N}_2)\}\text{Al}(\text{C}_6\text{F}_5)_3]$. The boron and aluminium adducts are structurally similar, showing a comparable level of N_2 push–pull activation. A notable exception is a bent (BCF adducts) vs. linear (AlCF adducts) $\text{M}-\text{N}-\text{N}-\text{LA}$ motif (LA = Lewis acid), explained computationally as the result of steric repulsion. A striking difference arose when the formation of two-fold adducts was conducted. While in the case of BCF the 2:1 Lewis pairs could be observed in equilibrium with the 1:1 adduct and free borane but resisted isolation, AlCF forms robust 2:1 adducts $\text{trans-}[\text{ML}_2(\mu-\eta^1:\eta^1-\text{N}_2)\text{Al}(\text{C}_6\text{F}_5)_3]_2$ that isomerise into a more stable *cis* configuration. These compounds could be isolated and structurally characterized, and represent the first examples of trinuclear heterometallic complexes formed by Lewis acid–base interaction exhibiting p and d elements. Calculations also demonstrate that from the bare complex to the two-fold aluminium adduct, substantial decrease of the HOMO–LUMO gap is observed, and, unlike the *trans* adducts (1:1 and 1:2) for which the HOMO was computed to be a pure d orbital, the one of the *cis*-trinuclear compounds mixes a d orbital with a π^* one of each N_2 ligands. This may translate into a more favourable electrophilic attack on the N_2 ligands instead of the metal centre, while a stabilized N_2 -centered LUMO should ease electron transfer, suggesting Lewis acids could be co-activators for electro-catalysed N_2 reduction. Experimental UV-vis spectra for the tungsten family of compounds were compared with TD-DFT calculations (CAM-B3LYP/def2-TZVP), allowing to assign the low extinction bands found in the visible spectrum to unusual low-lying MLCT involving N_2 -centered orbitals. As significant red-shifts are observed upon LA coordination, this could have important implications for the development of visible light-driven nitrogen fixation.

Received 24th April 2024

Accepted 14th June 2024

DOI: 10.1039/d4sc02713b

rsc.li/chemical-science

Introduction

Since the discovery of the first transition metal (TM) dinitrogen complex in 1965,¹ the quest for an efficient and mild process for dinitrogen transformation embodies an ultimate goal for chemists. Although much progress has been made in the last two decades in the field of artificial nitrogen fixation, the number of catalytic systems for N_2 conversion under

homogeneous conditions remains limited.^{2,3} Therefore, new molecular design strategies must be explored to overcome the current scientific barriers and to gain access to optimised N_2 conversion.

Donor–acceptor activation is a strategy that has not been largely implemented in N_2 chemistry involving molecular complexes. This parallels neither its success for other small molecules activation, *e.g.*, CO_2 ^{4–6} or H_2 ,^{7–9} both well exemplified through frustrated Lewis pair (FLP) chemistry^{10–17} and metal-ligand cooperativity,^{18,19} nor the fact that this concept finds echo in the two main processes responsible for nitrogen fixation. With regard to the nitrogenase enzymes, the “push–pull hypothesis” surmises that the acidic residues found in the active site build H-bonds with the distal N of N_2 bound to the FeMo-cofactor,^{20–24} thus increasing polarization of the diatomic molecule and facilitating its protonation.^{25,26} Besides, promotion of the Haber–Bosch catalysts with electropositive elements

^aLCC-CNRS, Université de Toulouse, CNRS, UPS 205 Route de Narbonne, BP44099, F-31077 Toulouse Cedex 4, France. E-mail: antoine.simonneau@lcc-toulouse.fr

^bDepartment of Chemistry, Quantum Chemistry, TU Darmstadt, Peter-Grünberg-Str. 4, 6, 4287 Darmstadt, Germany

† Electronic supplementary information (ESI) available: General methods, experimental procedures, NMR spectra, crystallographic and computational details and CIF files. CCDC 2346952–2346961. For ESI and crystallographic data in CIF or other electronic format see DOI: <https://doi.org/10.1039/d4sc02713b>



lowers the barrier for N_2 dissociation due to electrostatic effects, which can be seen as another manifestation of N_2 donor-acceptor activation.^{27–30}

At the molecular level, it can be achieved by the Lewis acid-base pairing of terminal N_2 complexes with Lewis acids,^{31–33} which results in increased N_2 polarisation due to enhanced back-bonding from the donor metal. This was pioneered by the Chatt group^{34–36} with neutral main-group Lewis acids, and was later further exemplified by the Fryzuk,³⁷ Tuczek,³⁸ Szymczak²⁵ and Simonneau^{39,40} groups. Main group^{41,42} and transition metal cations⁴³ have also been shown to participate in such type of donor-acceptor systems. The “donor” partner is generally an early-to-mid transition metal with a low formal oxidation state, although a model of purely main-group N_2 donor-acceptor activation system was proposed by the Stephan group.⁴⁴ By providing an access to a highly polarised N_2 unit, opportunities for the discovery of new reactivity patterns for dinitrogen complexes can arise, for instance N_2 protonation,²⁵ silylation or borylation.³⁹ In this context, the team of Szymczak and ours have focused on the coordination of the strong boron Lewis acid tris(pentafluorophenyl)borane, $\text{B}(\text{C}_6\text{F}_5)_3$ (**BCF**) with a series of group 6 and 8 ($\text{M} = \text{Mo}, \text{W}$, and Fe) phosphine N_2 -complexes and have studied with DFT the implications for the N_2 ligand.^{25,39,43} We have recently shown in a computational study that binding LAs to transition-metal N_2 -complexes may shift their molecular orbital ordering.⁴⁵ Thus, by levelling basicity and redox potentials, Lewis acid coordination to the N_2 ligand may be an interesting way to mitigate overpotentials in homogeneous ammonia synthesis (electro)catalysed with metal complexes. Recently, we turned our interest towards Lewis Super Acids (LSA),⁴⁶ driven by the curiosity of gauging the push-pull effect when the acceptor is an extremely electron-deficient species. We have shown that a two-channel activation by the means of a strongly electrophilic bis(borane) $\text{C}_6\text{F}_4\{\text{B}(\text{C}_6\text{F}_5)_2\}_2$ (**B₂CF**) imparts significant activation to the diatomic molecule, up to the diazene-diide (N_2^{2-}) state.⁴⁰ In the continuation of this work, we decided to study the coordination of the aluminium analogue of **BCF**, tris(pentafluorophenyl)alane – $\text{Al}(\text{C}_6\text{F}_5)_3$ (**AlCF**)^{47–56} – to group 6 dinitrogen complexes, in order to assess how the resulting Lewis pairs differ or not in terms of structure and reactivity with respect to **BCF**.

AlCF is structurally close to **BCF** as they both feature three C_6F_5 ligands in their coordination sphere and a central trivalent group 13 element, differing by their metal radii and electronegativity.⁵⁷ This apparently anecdotic distinction turns out to change quite significantly their chemical properties. As a matter of fact, while **BCF** is notably stable in a trigonal planar geometry and do not interact with weak and even moderate donors (such as non-polar and aromatic molecules and even oxygen-based compounds),^{58,59} **AlCF** is highly reactive (thermal and shock sensitive) in this configuration and is only stable in a tetrahedral environment where the 4th position is occupied by a weak donor^{49,51,53,60} or, in its unsolvated dimeric form, through double Al-F interactions between Al and the *ortho*-F atom of one C_6F_5 ring.⁵³ This singular aspect to form adducts with very weak donors (*vide infra*) suggests indeed higher electrophilic properties of **AlCF** vs. **BCF**, and it is now widely accepted that **AlCF** has

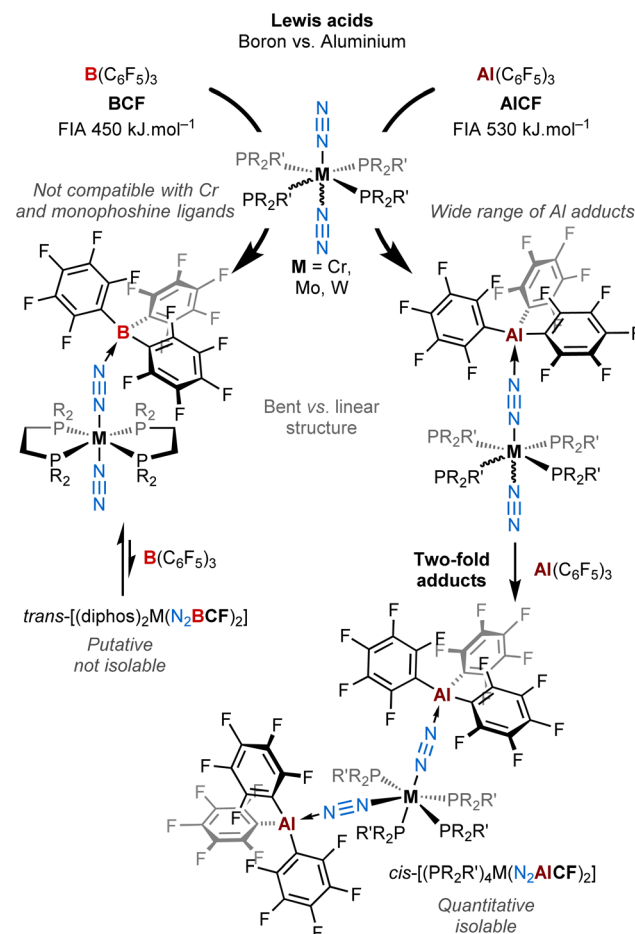


Fig. 1 Coordination of **AlCF** versus **BCF** on Group 6 end-on dinitrogen complexes leading to a new family of mono and double Al dinitrogen adducts.

a much stronger Lewis acid character than **BCF**.⁵⁶ From computational studies and compiled experimental data, **AlCF** is considered as an LSA, having a Fluoride Ion Affinity (FIA)⁶¹ – acknowledged to be a way to estimate Lewis acidity – of 530 kJ mol^{-1} . In ascending order, the latter has an FIA higher than **B₂CF** (523 kJ mol^{-1}), SbF_5 (490 kJ mol^{-1}) (the reference of the LSA scale), and much higher than **BCF** (450 kJ mol^{-1}).^{53,56,62–65}

In this work, we describe a new family of **AlCF** adducts with Chatt-Hidai type group 6 dinitrogen complexes, by the means of spectroscopy (NMR, IR, UV-vis), single crystal X-ray diffraction (sc-XRD), and DFT calculations. Notable chemical and structural discrepancies are observed by comparison to **BCF** (see Fig. 1), which are duly highlighted throughout the article. Remarkably, the switch from boron to aluminium allowed us to isolate bis(μ - η^1 : η^1 - N_2 -**AlCF**) adducts that remained elusive in the case of **BCF**. These are the first examples of neutral two-fold adducts of a main group Lewis acid with a bis(dinitrogen) complex.

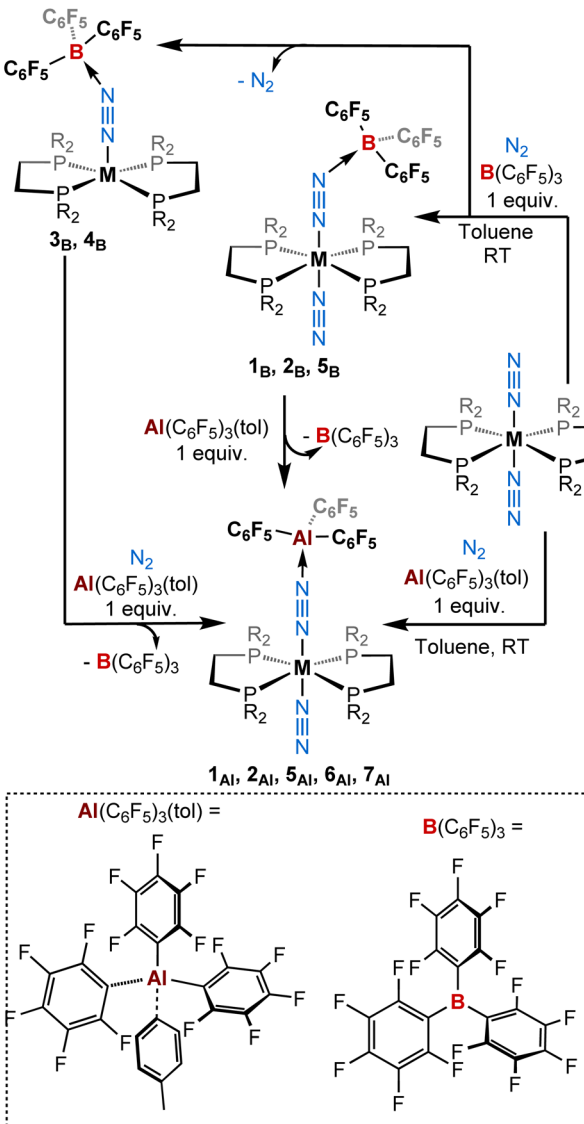
Results and discussion

Syntheses of 1:1 adducts supported with bis(phosphines)

Stoichiometric treatment (1:1) of tris(pentafluorophenyl)alane toluene adduct⁵¹ with a series of dinitrogen complexes *trans*-



[$\text{ML}_2(\text{N}_2)_2$] in toluene ($\text{M} = \text{W, Mo, and Cr}$; $\text{L} = 1,2\text{-bis(diethylphosphino)ethane [depe] or 1,2-bis(diphenylphosphino)ethane [dppe] or 1,2-bis(dimethylphosphino)ethane [dmpe]}$)^{43,66-75} under a dinitrogen atmosphere produced new 1:1 adducts [$\text{ML}_2(\text{N}_2)(\mu\text{-N}_2)\text{Al}(\text{C}_6\text{F}_5)_3$] $\mathbf{1}_{\text{Al}}$, $\mathbf{2}_{\text{Al}}$, $\mathbf{5}_{\text{Al}}$, $\mathbf{6}_{\text{Al}}$, and $\mathbf{7}_{\text{Al}}$ of *trans* configuration in moderate to excellent yields (Scheme 1 and Table 1). Note that better results in terms of analytical purity, yields, and reproducibility have been obtained with the depe and dmpe series (see ESI†). Adducts $\mathbf{1}_{\text{Al}}$, $\mathbf{2}_{\text{Al}}$, $\mathbf{5}_{\text{Al}}$, $\mathbf{6}_{\text{Al}}$ and $\mathbf{7}_{\text{Al}}$ were characterised in solution and in the solid-state by multi-nuclei NMR and IR spectroscopies as well as single-crystal XRD analysis. Similarities are found between the depe-supported complexes $\mathbf{1}_{\text{Al}}$, $\mathbf{2}_{\text{Al}}$ and their boron analogues $\mathbf{1}_{\text{B}}$, $\mathbf{2}_{\text{B}}$. Indeed, NMR signatures of these species are very close especially when considering their ^{31}P NMR resonance (see Table 3). Coordination of the LA (**BCF** or **AlCF**) at the distal nitrogen of the N_2 fragment induces a nearly equal bathochromic shift of the $\mu\text{-N}_2$



Scheme 1 Reactivity of $\text{ML}_2(\text{N}_2)_2$ ($\text{M} = \text{W, Mo, Cr}$; $\text{L} = \text{depe, dppe, dmpe}$) complexes with (top) $\text{B}(\text{C}_6\text{F}_5)_3$ and (bottom) $\text{Al}(\text{C}_6\text{F}_5)_3(\text{tol})$ (1 equiv.) under a dinitrogen atmosphere.

Table 1 Description of the different adducts

Compound	LA ^a	M	R	Config.	N_2 motifs	Yield (%)
$\mathbf{1}_{\text{Al}}$	AlCF	W	Et	trans	$\mu\text{-N}_2, \eta\text{-N}_2$	89
$\mathbf{1}_{\text{B}}^{43}$	BCF	W	Et	trans	$\mu\text{-N}_2, \eta\text{-N}_2$	62
$\mathbf{2}_{\text{Al}}$	AlCF	Mo	Et	trans	$\mu\text{-N}_2, \eta\text{-N}_2$	100
$\mathbf{2}_{\text{B}}^{43}$	BCF	Mo	Et	trans	$\mu\text{-N}_2, \eta\text{-N}_2$	53
$\mathbf{3}_{\text{B}}$	BCF	W	Ph	trans	$\mu\text{-N}_2$	{31} ^b
$\mathbf{4}_{\text{B}}$	BCF	Mo	Ph	trans	$\mu\text{-N}_2$	{95} ^b
$\mathbf{5}_{\text{Al}}$	AlCF	W	Ph	trans	$\mu\text{-N}_2, \eta\text{-N}_2$	51
$\mathbf{5}_{\text{B}}$	BCF	W	Ph	trans	$\mu\text{-N}_2, \eta\text{-N}_2$	{69} ^b
$\mathbf{6}_{\text{Al}}$	AlCF	Mo	Ph	trans	$\mu\text{-N}_2, \eta\text{-N}_2$	81
$\mathbf{7}_{\text{Al}}$	AlCF	Cr	Me	trans	$\mu\text{-N}_2, \eta\text{-N}_2$	79

^a LA = Lewis acid. ^b NMR yield.

$\text{N}\equiv\text{N}$ IR band and hypsochromic shift of the terminal $\text{N}\equiv\text{N}$ stretching mode (see Table 3).

Suitable single-crystals of $\mathbf{1}_{\text{Al}}$ and $\mathbf{2}_{\text{Al}}$ for XRD studies have been grown from a cold and saturated solution of toluene/*n*-pentane. The solid-state structures of $\mathbf{1}_{\text{Al}}$ and $\mathbf{2}_{\text{Al}}$ (see Fig. 3, left, for $\mathbf{1}_{\text{Al}}$ and ESI† for $\mathbf{2}_{\text{Al}}$) depict a similar octahedral geometry around the group 6 metal to that of $\mathbf{1}_{\text{B}}$ and $\mathbf{2}_{\text{B}}$. Expectedly, coordination of AlCF to the distal N atom in complexes $\mathbf{1}_{\text{Al}}$ and $\mathbf{2}_{\text{Al}}$ imparts a tetrahedral geometry around the Al center (angles averaged at 109.5° for $\mathbf{1}_{\text{Al}}$ and 108.0° for $\mathbf{2}_{\text{Al}}$). The $\text{N}_1\text{-N}_2$ bond lengths are similar between the aluminium and boron analogues (see Table 3). The TM-N₁ distance is slightly shortened in the case of aluminium adducts ($\text{W-N}_1 = 1.855 \text{ \AA}$ for $\mathbf{1}_{\text{Al}}$ vs. 1.909 \AA for $\mathbf{1}_{\text{B}}$ and $\text{Mo-N}_1 = 1.869 \text{ \AA}$ for $\mathbf{2}_{\text{Al}}$ vs. 1.894 \AA for $\mathbf{2}_{\text{B}}$).

Overall, these experimental data point to a diminished bond order for the N_2 unit as a result of enhanced back-donation with a similar “push-pull” activation level of $\mu\text{-N}_2$ in species $\mathbf{1}_{\text{Al}}$, $\mathbf{2}_{\text{Al}}$ and $\mathbf{1}_{\text{B}}$, $\mathbf{2}_{\text{B}}$. However, we noticed structural divergences between $\mathbf{1}_{\text{Al}}$, $\mathbf{2}_{\text{Al}}$ and their boron analogues $\mathbf{1}_{\text{B}}$, $\mathbf{2}_{\text{B}}$. According to the Cambridge Structural Database (CSD), the $\text{Al}_1\text{-N}_2$ bond lengths – 1.817 \AA for $\mathbf{1}_{\text{Al}}$ and 1.842 \AA for $\mathbf{2}_{\text{Al}}$ – are found to be the shortest ones compared to the expected Al-N distances range for similar reported $\text{N-Al}(\text{C}_6\text{F}_5)_3$ motifs (from 1.853 \AA ^{76,77} to 2.167 \AA ⁷⁸) and $\text{N}_2\text{-AlR}_3$ ($\text{R} = \text{alkyl}$) fragments (from 1.929 \AA ⁷⁹ to 2.089 \AA ⁸⁰). On the other hand, the B-N₂ length for the boron congeners (1.549 \AA for $\mathbf{1}_{\text{B}}$ and 1.562 \AA for $\mathbf{2}_{\text{B}}$) are found in the expected B-N distances range for similar reported $\text{N-B}(\text{C}_6\text{F}_5)_3$ moieties (from 1.492 \AA ⁸¹ to 1.807 \AA ⁸²) but are slightly below the B-N distances range for comparable bridging diazo borane ($\mu\text{-N}_2\text{-B}(\text{C}_6\text{F}_5)_3$) and azido borane ($\mu\text{-N}_3\text{-B}(\text{C}_6\text{F}_5)_3$) fragments (from 1.575 \AA ²⁵ to 1.678 \AA ³⁸). These results thus advocate for the presence of robust interactions between the bridging N_2 and the LA centre, more prominent in the case of aluminium.

Experimentally, we demonstrated the stronger affinity of $\mu\text{-N}_2$ motif for AlCF vs. BCF by treating adduct $\mathbf{1}_{\text{B}}$ with one equivalent of $\text{Al}(\text{C}_6\text{F}_5)_3(\text{tol})$ that leads to the formation of $\mathbf{1}_{\text{Al}}$ and free BCF with an NMR yield higher than 90% (see Scheme 1 and ESI†). Note that over time this equilibrium does not evolve showing that the formation of $\mathbf{1}_{\text{Al}}$ from $\mathbf{1}_{\text{B}}$ is thermodynamically favourable. This set of clues led us to analyse the $\text{N}_1\text{-N}_2\text{-LA}$ angle. In the case of the aluminium adducts, a nearly straight

$\text{N}_1\text{-N}_2\text{-Al}$ angle is found – 168.4° and 167.8° for $\mathbf{1}_{\text{Al}}$ and $\mathbf{2}_{\text{Al}}$, respectively. These data conflict with similar reported $\text{N}=\text{N}-\text{Al}$ angles of bridging diazenido trialkylaluminum ($\mu\text{-N}=\text{N}-\text{AlR}_3$) and azido trialkylaluminum ($\mu\text{-N}=\text{N}=\text{N}-\text{AlR}_3$) species featuring values ranging from 105.5° ⁸⁰ to 158.9° .⁸⁴ These results also contrast with the bent $\text{N}_1\text{-N}_2\text{-B}$ angle found for the boron analogues – 148.4° for $\mathbf{1}_{\text{B}}$ and 150.9° for $\mathbf{2}_{\text{B}}$. While $[\text{M}(\text{depe})_2(\text{N}_2)_2]$ and $[\text{M}(\text{dppe})_2(\text{N}_2)_2]$ cleanly reacted with **BCF** to form quantitatively 1:1 adducts, we observed significant divergent behaviours when we engaged *trans*- $[\text{Cr}(\text{dmpe})_2(\text{N}_2)_2]$ with **BCF**. Indeed, this leads to a partial and unselective reaction towards a complex mixture of species (starting materials in equilibrium with other species, see ESI†) that we were not able to isolate from each other in the solid-state. Among them, we can assume that the 1:1 adduct is partly formed. On the opposite, the stoichiometric reaction of $\text{Al}(\text{C}_6\text{F}_5)_3(\text{tol})$ with $[\text{Cr}(\text{dmpe})_2(\text{N}_2)_2]$ cleanly produced a new 1:1 adduct $\mathbf{7}_{\text{Al}}$ in good yields (Scheme 1, bottom). Spectroscopic and crystallographic parameters of $\mathbf{7}_{\text{Al}}$ are nearly identical to those of tungsten and molybdenum analogues $\mathbf{1}_{\text{Al}}$ and $\mathbf{2}_{\text{Al}}$ (see Fig. 3 and Table 3) showing a similar N_2 activation degree (close N-N distances and $\text{N}\equiv\text{N}$ IR stretches) and **AlCF** coordination (close Al-N distances and Al-N-N angles in particular).

DFT investigation on the N-N-LA angle

To shed light into these results, DFT calculations at the BP86/def2-TZVP level of theory were employed, including implicit solvation and dispersion corrections, starting from the crystal structures of the **BCF** and **AlCF** adducts. One explicit solvent molecule was added to the molecular models due to the aforementioned greater stability of **AlCF** in a tetrahedral environment; this is required for the analysis of the thermodynamics behind the LA binding.

The potential energy surface (PES) minima found upon geometry relaxation match well with experiment: M-N_1 and $\text{N}_2\text{-LA}$ bonds were only *ca.* 0.050 \AA longer than the experimental ones and other deviations were even smaller. The $\text{N}_1\text{-N}_2\text{-LA}$ angles obtained for the computed structures of **AlCF** and **BCF** adducts were 170° and 148° , respectively. A detailed comparison of the computational and experimental structural and spectroscopic features is included in the ESI (Tables S5 and S6).† To further elucidate the PES regarding the binding angle of the LAs, constrained geometry optimisations with varying N-N-LA angles (148° to 172°) were carried out for both LA adducts (Fig. 2). The $\text{N}\equiv\text{N-B}$ angle is in fact extremely flexible: in the case of the least sterically impeded adduct, we observe the energy minimum at *ca.* 150° (in agreement with experimental data) and a small dent close to 165° , separated by less than 0.5 kcal mol^{-1} . The latter is not a local minimum as it is due to a *ca.* 10° rotation of one ethyl phosphine substituent. The increase in energy along the bending motion is, overall, meagre, with an energetic cost of less than 1 kcal mol^{-1} . For the **AlCF** 1:1 adduct, in contrast, a continuous and steeper increase in energy is observed as the $\text{N}\equiv\text{N-LA}$ angle is decreased.

There is a marginal stabilisation of the frontier occupied orbitals in both adducts as the angle is bent from 148° to 172° .

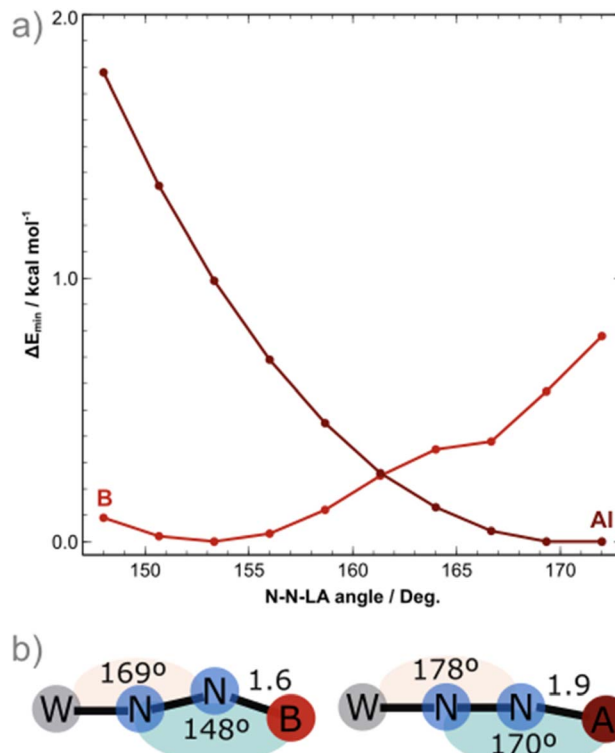


Fig. 2 (a) Potential energy surface along the $\text{N-N-Lewis$ acid angle coordinate for the **AlCF** (crimson) and **BCF** (red) 1:1 adducts, energies reported relative to PES minimum; and (b) relevant angles of the optimized structures.

(Fig. S93†), suggesting that the differing angles obtained in the crystal structures are not rooted in electronic structure stabilisation effects but are instead mainly due to steric hindrances. Note that for the $\text{N}\equiv\text{N-LA}$ angle to bend (blue in Fig. 1b), a simultaneous bending of the $\text{M-N}_1\equiv\text{N}_2$ angle (peach, in Fig. 1b) by 9° occurs to better accommodate the LA around the phosphine ligand arms. This is true for both LAs.

Influence of the atmosphere: N_2 vs. Ar

It is important to mention that for adducts in the **depe** and **dmpe** series we observed the same reactivity whether working under dinitrogen or argon. Nevertheless, we noticed significant divergences for the **dppe** series. Indeed, when using $\text{B}(\text{C}_6\text{F}_5)_3$, our group had previously observed the elimination of one dinitrogen molecule during the reaction leading to the formation of $[\text{M}(\text{dppe})_2(\mu\text{-N}_2)\text{B}(\text{C}_6\text{F}_5)_3]$ adducts where the apical site (left vacant by N_2 dissociation) is occupied by an *ortho* hydrogen of one of the phenyl groups in the solid-state.³⁹ This process occurred under argon (Scheme 2, middle). Under dinitrogen, we noticed the same reactivity for *trans*- $[\text{Mo}(\text{dppe})_2(\text{N}_2)_2]$ (*i.e.* loss of one of the N_2 ligands) but the stoichiometric treatment of *trans*- $[\text{W}(\text{dppe})_2(\text{N}_2)_2]$ with **BCF** leads, after one night, to a mixture of $[\text{W}(\text{dppe})_2(\mu\text{-N}_2)\text{B}(\text{C}_6\text{F}_5)_3]$ $\mathbf{3}_{\text{B}}$ and *trans*- $[\text{W}(\text{dppe})_2(\text{N}_2)(\mu\text{-N}_2)\text{B}(\text{C}_6\text{F}_5)_3]$ $\mathbf{5}_{\text{B}}$ in a $31:69\text{ } \mathbf{3}_{\text{B}}:\mathbf{5}_{\text{B}}$ ratio, respectively. Of note, species $\mathbf{5}_{\text{B}}$ was observed in solution but we did not succeed to isolate it (see Scheme 1, top left, and ESI†).



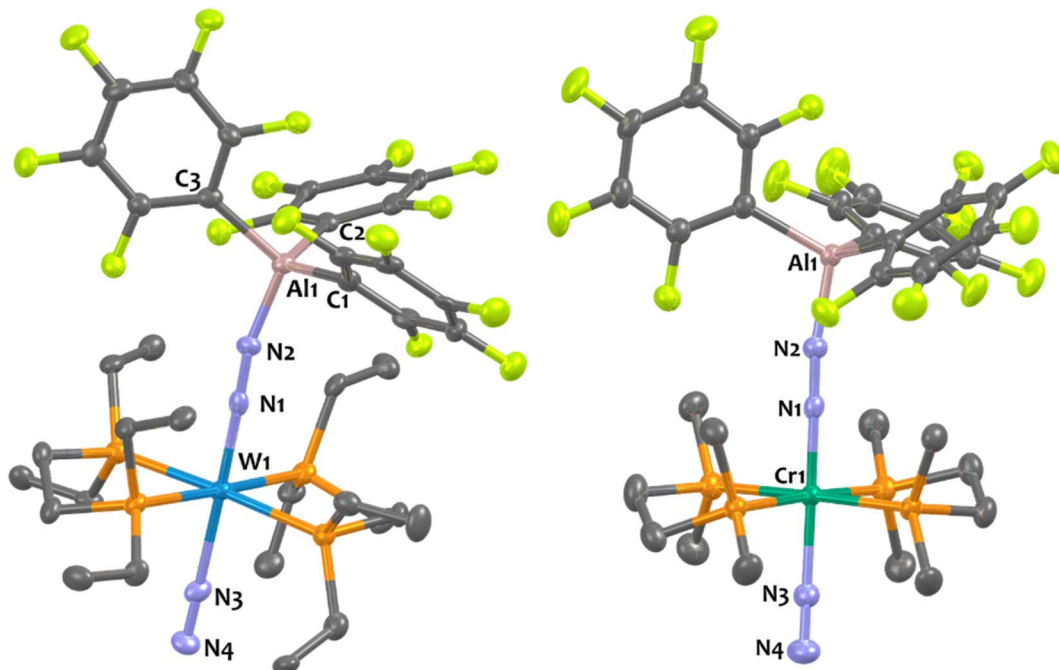


Fig. 3 Solid-state structures of 1_{Al} and 7_{Al} . Ellipsoids are represented with 30% probability. Hydrogen atoms have been omitted for clarity. Two independent molecules were found in the asymmetric unit ($Z' = 2$) of 1_{Al} but one of them has been omitted for clarity. Selected bond distances (\AA) and angles ($^{\circ}$) have been averaged between both independent molecules for 1_{Al} : Al_1-N_2 1.816(7), W_1-N_1 1.855(2), W_1-N_3 2.113(2), N_1-N_2 1.203(6), N_3-N_4 1.114(1), $\text{W}_1-\text{N}_1-\text{N}_2$ 178.6(6), $\text{W}-\text{N}_3-\text{N}_4$ 177.2(6), $\text{N}_1-\text{W}_1-\text{N}_3$ 177.3(6), $\text{N}_1-\text{N}_2-\text{Al}_1$ 168.3(6). For 7_{Al} : Al_1-N_2 1.8473, Cr_1-N_1 1.7507, Cr_1-N_3 1.9766, N_1-N_2 1.177(2), N_3-N_4 1.100(3), $\text{N}_3-\text{Cr}_1-\text{N}_1$ 177.47(7), $\text{N}_2-\text{N}_1-\text{Cr}_1$ 178.55(2), $\text{N}_4-\text{N}_3-\text{Cr}_1$ 178.02(18), $\text{N}_1-\text{N}_2-\text{Al}_1$ 170.26(2).

By contrast, the reaction of $\text{Al}(\text{C}_6\text{F}_5)_3$ with *trans*- $[\text{M}(\text{dppe})_2(\text{N}_2)_2]$ ($\text{M} = \text{Mo}$ and W) does not promote the elimination of N_2 when working under a dinitrogen atmosphere. This leads instead to a similar reactivity to that of the depe series *i.e.* the formation of products 5_{Al} and 6_{Al} where the terminal N_2 stays bonded to the metal centre (Scheme 1). Under an inert atmosphere of argon, the stoichiometric treatment of AlCF with *trans*- $[\text{Mo}(\text{dppe})_2(\text{N}_2)_2]$ leads predominantly (73% NMR yield, see ESI[†]) to the formation of the aluminium analogue of 4_{B} , $[\text{Mo}(\text{dppe})_2(\mu-\text{N}_2)\text{AlCF}]$ 4_{Al} , in which the second dinitrogen ligand is lost during the reaction (Scheme 2, top). Identity of adduct 4_{Al} is successfully established by XRD studies. It should be noted, however, that the quality of XRD data was not good enough to discuss the metrical parameters in great detail but confirmed the atom connectivity and loss of one N_2 ligand (see ESI[†]).

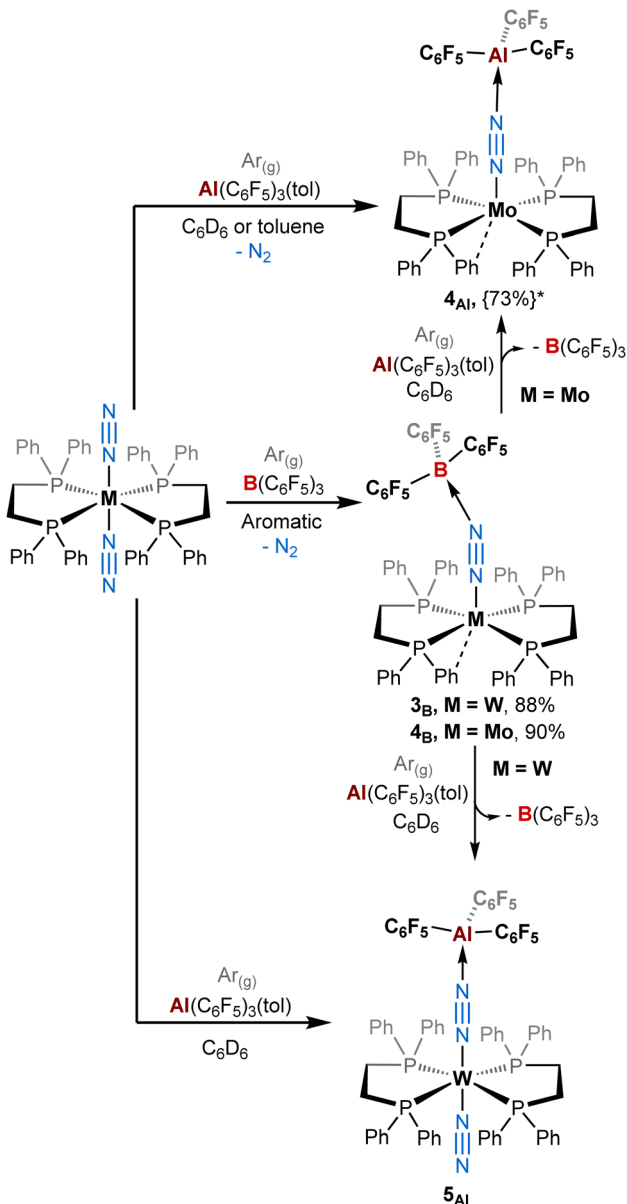
Surprisingly, changing from Mo to W drastically impacts this chemistry since the 1 : 1 reaction of *trans*- $[\text{W}(\text{dppe})_2(\text{N}_2)_2]$ with AlCF under argon does not trigger N_2 dissociation and instead promotes the quantitative formation of 5_{Al} as under a dinitrogen atmosphere (see Scheme 2, bottom, and ESI[†]). This highlights the sensitivity of these species towards the retention of their second N_2 ligand, depending whether the reaction medium is N_2 -saturated or not. We assumed that formation of adducts 3–4 involves first the formation of 5–6 as intermediates (coordination of the LA at the distal N), which can then lose their terminal N_2 ligand depending on the LA and the atmosphere. In this case, this second step is more feasible (in ascending order) for $4_{\text{B}} > 3_{\text{B}} > 4_{\text{Al}} > 3_{\text{Al}}$. This translates into Mo-

and/or B-containing species having a greater tendency to labilise the *trans*- N_2 ligand. Spectroscopic and crystallographic data of 3–4 vs. 5–6 revealed distinct features (Table 3). The IR $\mu\text{-N}\equiv\text{N}$ stretching mode is shifted to lower wavenumbers for adducts 3–4 vs. 5–6 and the bridging N–N distances are elongated in adducts 3–4 vs. 5–6. Therefore, the elimination of the terminal dinitrogen molecule induces a stronger polarisation of the M– $\text{N}\equiv\text{N}$ –LA fragment (3_{B} , 4_{B} vs. 5_{Al} and 6_{Al}). Notably, comparable crystallographic data between 5_{Al} , 6_{Al} and 1_{Al} , 2_{Al} are found when it comes to the LA– N_2 distance and N_1-N_2 –LA angle *i.e.* a short Al–N separation and a nearly linear Al– $\text{N}\equiv\text{N}$ array, again contrasting with the boron adducts 3_{B} and 4_{B} featuring bent B– $\text{N}\equiv\text{N}$ angles (see Table 3).

Also, similarly to the depe series, the stronger affinity of N_2 metal complexes for AlCF vs. BCF in the dppe series was verified experimentally by treating the BCF adducts $3_{\text{B}}\text{--}4_{\text{B}}$ with one equivalent of AlCF producing instantly (whether working under argon or dinitrogen) the aluminium adducts 4_{Al} , 5_{Al} , and 6_{Al} and free BCF (see Scheme 1, left, Scheme 2, and ESI[†]). These reactions demonstrate the stronger affinity of AlCF vs. BCF for the dinitrogen ligand.

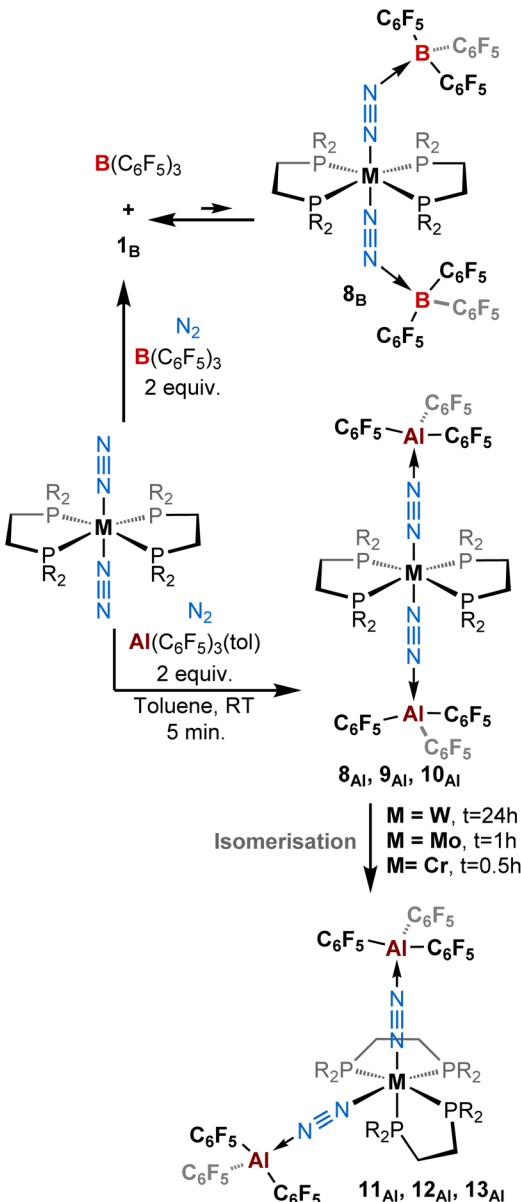
Syntheses of 2 : 1 adducts

Since we employed bis(dinitrogen) complexes as Lewis base partner, we were curious to know whether the reaction of $[\text{ML}_2(\text{N}_2)_2]$ with two equivalents of the Lewis acid (AlCF or BCF) could provide 2 : 1 adducts. When we added two equivalents of $\text{B}(\text{C}_6\text{F}_5)_3$ to $[\text{M}(\text{depe})_2(\text{N}_2)_2]$ ($\text{M} = \text{Mo}$, W) we noticed an



Scheme 2 Reactivity of $ML_2(N_2)_2$ ($M = W, Mo$; $L = dppe$) complexes with $B(C_6F_5)_3$ and $Al(C_6F_5)_3(tol)$ under an argon atmosphere. {The yield in brackets followed by a star*} represents the NMR yield. The other complexes ($L = depe$ or $dmpe$) reacted similarly as under a dinitrogen atmosphere (see Scheme 1).

immediate colour change from orange-brown to deep purple-blue. While in the case of molybdenum, NMR analyses suggested some degradation occurring upon addition of the second equivalent of BCF, the spectra recorded when the W species was employed suggests the formation of a new putative complex 8_B (see Scheme 3, top, and Table 2). This is evidenced by a gain in symmetry as indicated by undifferentiated alkyl protons in the 1H NMR spectrum, as opposed to 1_B (see ESI[†]). However, we also cannot exclude that such 1H NMR spectrum results from signal coalescence of 1_B due to a concentration phenomenon as already observed in the case of 1_{AI} (Fig. S1–S3 and S40[†]). This



Scheme 3 Reactivity of $[ML_2(N_2)_2]$ ($M = W, Mo, Cr$; $L = depe, dppe, dmpe$) complexes with (top) two equivalents of $B(C_6F_5)_3$ and (bottom) two equivalents of $Al(C_6F_5)_3(tol)$ under a dinitrogen atmosphere.

could explain why the ^{31}P NMR spectrum showed no change with respect to the mono adduct 1_B ($\delta = 34.7$ ppm). Surprisingly, only two large signals are observed in ^{19}F NMR, contrasting with the well-resolved multiplets characterizing *ortho*, *meta* and *para* fluorine resonances in 1_B . This may suggest either a fluxional behaviour of 8_B or that a fast $1_B + BCF \rightleftharpoons 8_B$ equilibrium takes place at room temperature. Measuring 1H and ^{19}F NMR at low temperature (down to $-60^\circ C$) resulted in de-coalescence of the signals. In particular, broad resonances, which chemical shifts match those of 1_B and free BCF, are found in the ^{19}F NMR spectrum, pointing to an equilibrated mixture. Shoulders on the peaks of the *para* and *meta* fluorine of 1_B might be assigned to the two-fold adduct 8_B (Scheme 1, top-right, and Fig. S40[†]).



Table 2 Description of the two-fold adducts

Compound	LA ^a	M	R	Config.	N ₂ motifs	Yield (%)
8 _{Al}	AlCF	W	Et	<i>trans</i>	2× μ-N ₂	96
8 _B	BCF	W	Et	<i>trans</i>	2× μ-N ₂	n.i. ^b
9 _{Al}	AlCF	Mo	Et	<i>trans</i>	2× μ-N ₂	n.i. ^b
10 _{Al}	AlCF	Cr	Me	<i>trans</i>	2× μ-N ₂	n.i. ^b
11 _{Al}	AlCF	W	Et	<i>cis</i>	2× μ-N ₂	77
12 _{Al}	AlCF	Mo	Et	<i>cis</i>	2× μ-N ₂	94
13 _{Al}	AlCF	Cr	Me	<i>cis</i>	2× μ-N ₂	77

^a LA = Lewis acid. ^b n.i. = not isolated.

Unfortunately, our attempts to isolate such a two-fold adduct were unsuccessful: crystals of **1_B** were systematically collected from the purple solutions.

Gratifyingly, treatment of *trans*-[M(depe)₂(N₂)₂] (M = Mo, W) and *trans*-[M(dmpe)₂(N₂)₂] (M = Cr) with two equivalents of AlCF·toluene instantly triggered a quantitative reaction characterised by a colour change from reddish (ML₂(N₂)₂ starting materials) to blue/azure/greenish within seconds. We attributed this colour change to the formation of a 2 : 1 adduct with a *trans*-configuration – species **8_{Al}** (M = W), **9_{Al}** (M = Mo), and **10_{Al}** (M = Cr) (Scheme 3, Table 2, and Fig. 4, top). With time, we noticed an additional colour change from blue/green to brown/orange corresponding to the formation of another 2 : 1 adduct this time with a *cis*-configuration, namely products **11_{Al}** (M = W), **12_{Al}** (M = Mo), and **13_{Al}** (M = Cr) (Scheme 3, bottom, and Fig. 4, bottom).

In the case of tungsten, intermediate **8_{Al}** is stable enough (for one or two hours at room temperature) so that we succeeded to

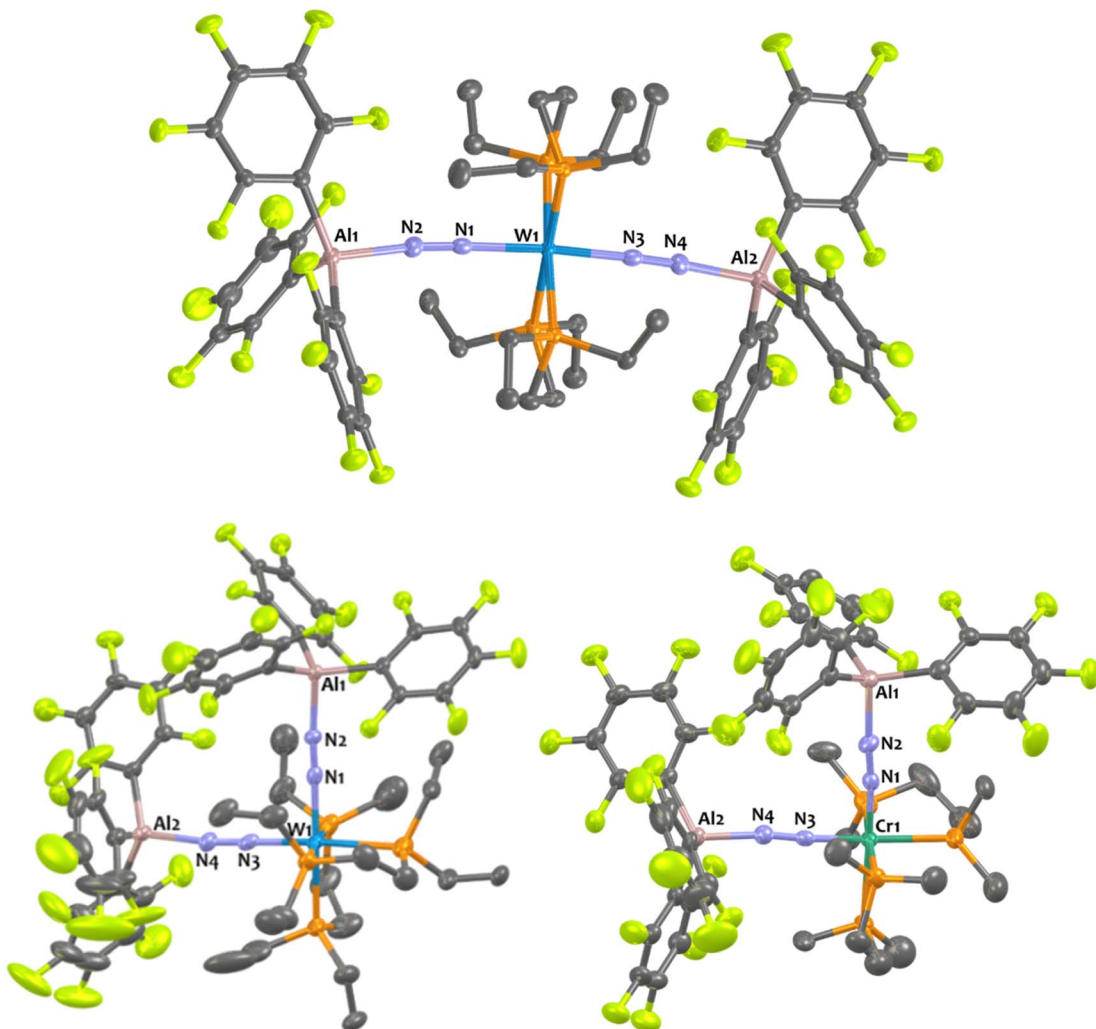


Fig. 4 Solid-state structures of **8_{Al}**, **11_{Al}**, and **13_{Al}**. Ellipsoids are represented with 30% probability. Hydrogen atoms have been omitted for clarity. Two independent molecules were found in the asymmetric unit ($Z' = 2$) of **11_{Al}** and **13_{Al}** but one of them has been omitted for clarity. Selected bond distances (Å) and angles (°) have been averaged between both independent molecules for **11_{Al}** and **13_{Al}**. For **8_{Al}**: Al₁–N₂ 1.927(2), Al₂–N₄ 1.919(2), W₁–N₁ 1.964(2), W₁–N₃ 1.956(3), N₁–N₂ 1.113(3), N₃–N₄ 1.114(3), N₃–W₁–N₁ 174.13(7), N₂–N₁–W₁ 176.88(2), N₄–N₃–W₁ 177.09(2), N₁–N₂–Al₁ 168.64(2), N₃–N₄–Al₂ 175.22(2). For **11_{Al}**: Al₁–N₂ 1.901(4), Al₂–N₄ 1.894(0), W₁–N₁ 1.919(9), W₁–N₃ 1.901(0), N₁–N₂ 1.144(6), N₃–N₄ 1.156(6), W₁–N₁–N₂ 175.5(4), W₁–N₃–N₄ 175.8(4), N₁–W₁–N₃ 89.20(7), Al₁–N₂–N₁ 175.7(9), Al₂–N₄–N₃ 168.7(4). For **13_{Al}** Al₁–N₂ 1.884(6), Al₂–N₄ 1.899(0), Cr₁–N₁ 1.784(2), Cr₁–N₃ 1.778(9), N₁–N₂ 1.156(1), N₃–N₄ 1.157(1), Cr₁–N₁–N₂ 175.6(9), Cr₂–N₃–N₄ 176.0(9), N₁–Cr₁–N₃ 89.19(2), Al₁–N₁–N₂ 170.8(4), Al₂–N₄–N₃ 172.0(0).



Table 3 Relevant structural and spectroscopic parameters (distances (Å), angles (°), wavenumbers (cm⁻¹), chemical shift (ppm)) of the aluminium and boron adducts

Adduct	δ ³¹ P NMR ^a	ν_1 (μ -N ₂)	ν_2 (N ₂)	N ₁ -N ₂	N ₃ -N ₄	N ₂ -LA ^b	N ₄ -LA ^b	M-N ₁	M-N ₃	N ₁ -M-N ₃	N ₁ -N ₂ -LA ^b	N ₃ -N ₄ -LA ^b
1_{Al}	34.6	1778	2088	1.204	1.114	1.817	—	1.855	2.113	177.4	168.4	—
1_B	34.7	1767	2076	1.181	1.082	1.549	—	1.909	2.015	175.7	148.4	—
2_{Al}	52.6	1790	2137	1.168	1.103	1.842	—	1.869	2.128	177.7	167.8	—
2_B	53.0	1789	2120	1.175	1.093	1.562	—	1.894	2.129	176.3	150.9	—
3_B	69.2	1717	—	1.212	—	1.571	—	1.841	—	—	140.3	—
4_{Al}	70.9	—	—	—	—	—	—	—	—	—	—	—
4_B	73.1	1744	—	1.197	—	1.568	—	1.841	—	—	141.5	—
5_{Al}	45.4	1773	2121	1.181	1.090	1.865	—	1.885	2.108	177.2	169.3	—
6_{Al}	63.1	1786	2161	1.174	1.094	1.876	—	1.894	2.139	173.8	176.6	—
7_{Al}	62.3	1802	2122	1.177	1.100	1.847	—	1.751	1.977	177.5	170.3	—
8_{Al}	31.0	1808	—	1.113	1.114	1.927	1.919	1.964	1.956	174.1	168.6	175.2
11_{Al}	28.6, 16.6	1903, 1802	—	1.145	1.157	1.901	1.894	1.920	1.901	89.2	175.8	168.7
12_{Al}	44.4, 29.2	1927, 1821	—	1.148	1.138	1.892	1.907	1.910	1.921	88.6	173.9	170.7
13_{Al}	—	1948, 1833	—	1.156	1.157	1.885	1.899	1.784	1.779	89.2	170.8	172.0
15_{Al}	-18.8, -22.1, -25.5	1776	2037	—	—	—	—	—	—	—	—	—
16_{Al}	-24.3, -26.5	1901, 1804	—	1.149	1.150	1.915	1.891	1.917	1.906	91.3	168.5	179.1

^a Recorded in C₆D₆. ^b LA = Lewis acid.

isolate it and analyse it by IR, XRD, and NMR. Then, **8_{Al}** is progressively (within one day) converted into product **11_{Al}**. However, intermediates **9_{Al}** (M = Mo) and **10_{Al}** (M = Cr) evolved within minutes towards products **12_{Al}** and **13_{Al}**, precluding their isolation (see ESI† for further details). The *trans* geometry of intermediate **8_{Al}** is first evidenced by its ¹H NMR spectrum that exhibits 3 centrosymmetric signals (δ = 1.44, 1.13, and 0.68 ppm) and by its ³¹P NMR spectrum that displays a shielded pseudo-triplet (J_{W-P} = 141 Hz) at δ = 31.0 ppm (vs. 34.6 ppm for **1_{Al}**). This configuration is confirmed by its structure in the solid-state (Fig. 4, top). Here, the Al₁-N₂-N₁-W₁-N₃-N₄-Al₂ atoms are almost perfectly aligned. Also, the coordination of a second AlCF moiety imparts a significant shortening of the N-N bonds (1.11 Å vs. 1.20 Å in **1_{Al}**) and elongation of the W-N₁ (1.96 Å vs. 1.86 Å in **1_{Al}**) and Al-N (1.92 Å vs. 1.82 Å in **1_{Al}**) bonds (see Table 3) showing a decreased activation of the bridging dinitrogen fragments. These features are verified by IR where the ATR spectrum of **8_{Al}** displays a single bridging N₂ stretch at higher wavenumber to that of **1_{Al}** (1808 vs. 1778 cm⁻¹). Based on these data, we propose a formal bridging Al-N≡N-M depiction. The *cis* arrangement of products **11_{Al}** and **12_{Al}** is first demonstrated by NMR spectroscopy as their ¹H NMR spectra display asymmetrical depe resonances (see Fig. S44 and S54†) and their ³¹P NMR spectra feature two triplets (J_{P-P} = 6 Hz and 14 Hz for **11_{Al}** and **12_{Al}**), each integrating for 2P (see Table 3 and ESI†). We could not analyse **13_{Al}** (M = Cr, L = dmpe) by NMR spectroscopy as this species was not soluble in chemically compatible deuterated solvents (even *ortho*-dichlorobenzene). IR-ATR spectra of **11_{Al}**, **12_{Al}**, and **13_{Al}** display two intense N≡N bands (see Table 3) assigned to symmetric and asymmetric N₂ stretches. Eventually, solid-state structures of **11_{Al}**, **12_{Al}**, and **13_{Al}** (see Fig. 4-bottom and ESI†) confirmed the *cis* arrangement, with almost orthogonal N₁-M-N₃ angles. Of note, an elongation of the N-N bond is observed for **11_{Al}** when compared to the *trans* adduct **8_{Al}** (1.152 Å vs. 1.113 Å, respectively).

DFT investigation on the 2 : 1 adduct formation

DFT calculations show that sequential binding of two equivalents of BCF or AlCF is thermodynamically favourable (Fig. 5), although binding of the second LA is associated with a relatively lower stabilisation of the adduct as may be expected from the *trans* effect. The individual contributions to the Gibbs energies can be found in the ESI, Tables S7 and S8.†

The AlCF adducts are lower in relative energy than the BCF analogues. Conversion from *trans* to *cis* adducts was observed and indeed the *cis* isomeric form is shown to be more stable by 3.0 kcal mol⁻¹ over the *trans* 2 : 1 adduct. We analysed the MO diagrams of the AlCF adduct series to rationalise the degree of dinitrogen activation observed (Fig. 6). The complete frontier MO diagram as well as the depiction of the orbitals for the bare tungsten depe complex can be found in the ESI (Fig. S92).†

The binding of LAs to the terminal atom of the nitrogen ligand has been shown to stabilise π^* interactions in the N-N

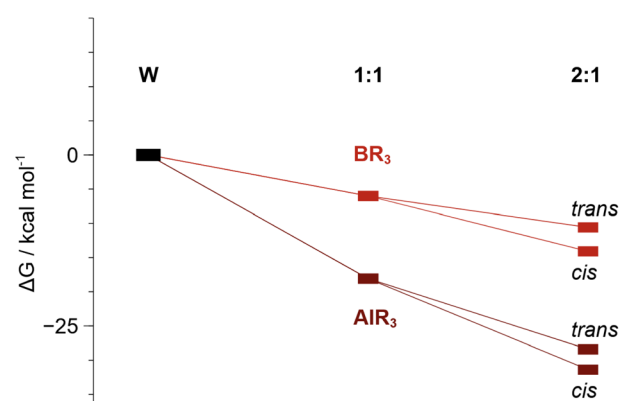


Fig. 5 Relative Gibbs energies (kcal mol⁻¹) of 1 : 1 (**1_B** and **1_{Al}**) and 2 : 1 adduct formation. The *cis* isomer is more stable than the *trans* by ca. 3 kcal mol⁻¹.



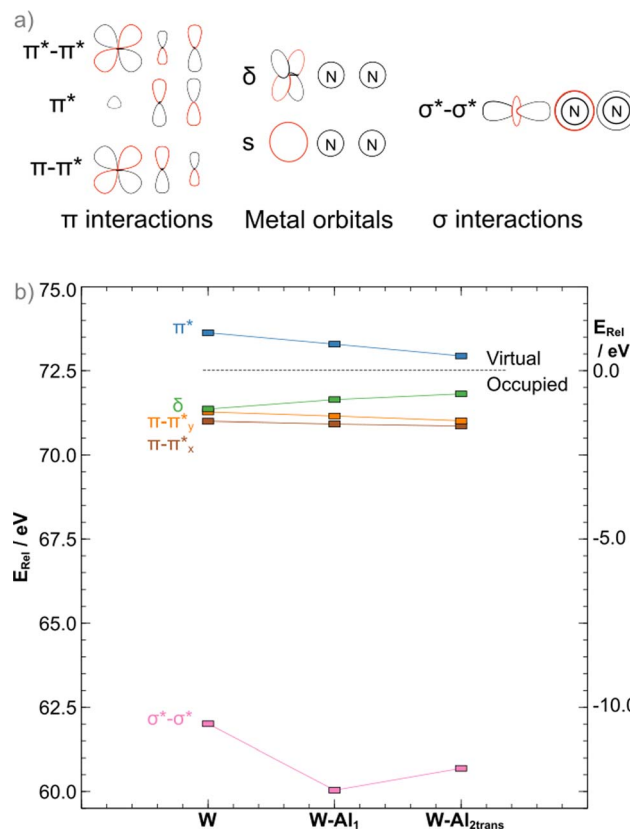


Fig. 6 (a) 2D depiction of the orbitals involved in the "push-pull" activation and metal s orbital used as reference and (b) MO diagram for the Al series of adducts (blue: LUMO/LUMO+1 average; green: HOMO; orange: HOMO-1; brown: HOMO-2; pink: σ antibonding interaction within the bridge). Orbital energies are plotted relative to the tungsten s orbital and thus all are positive (left vertical axis). Energies relative to proximally the midpoint of the HOMO/LUMO gap shown on the right vertical axis. Nomenclature of the orbitals considers symmetry.

bridge, resulting in bond²⁵ weakening. In the case of the depe complexes, the same is observed when the formation of the 1 : 1 adduct occurs as a *ca.* 0.10 eV stabilisation from the bare complex to the **AlCF** 1 : 1 adduct ($\nu_{\text{N-N}} = 1778 \text{ cm}^{-1}$) is observed. However, in apparent contradiction to experimental results ($\nu_{\text{N-N}} = 1808 \text{ cm}^{-1}$ measured for the 2 : 1 *trans* adduct), a further *ca.* 0.08 eV stabilisation is noted upon binding of the second LA. As we have shown in previous work,⁴⁵ an analysis of the π interactions is insufficient to explain dinitrogen activation in such complexes. A concomitant destabilisation (0.65 eV) of the $\sigma^*-\sigma^*$ orbital is observed that greatly exceeds the π stabilisation, explaining the increase in N–N stretching frequency (from the computed 1864 cm^{-1} in W-Al_1 to 1880 cm^{-1} in $\text{W-Al}_{2\text{trans}}$). The more stable *cis* adduct showed a slightly decreased bond strength ($\nu_{\text{N-N}} = 1802 \text{ cm}^{-1}$). The MO diagram for the *cis* 2 : 1 adduct shows a further 0.21 eV destabilisation of the $\sigma^*-\sigma^*$ orbital, which should result in a stronger dinitrogen bond. It is not the case here, however, as the different coordination geometry allows for mixing of the metal d orbital that would form the δ MO in the *trans* adducts with the π orbitals of the dinitrogen bridge (Fig. 7). Therefore, the nature of the HOMO –

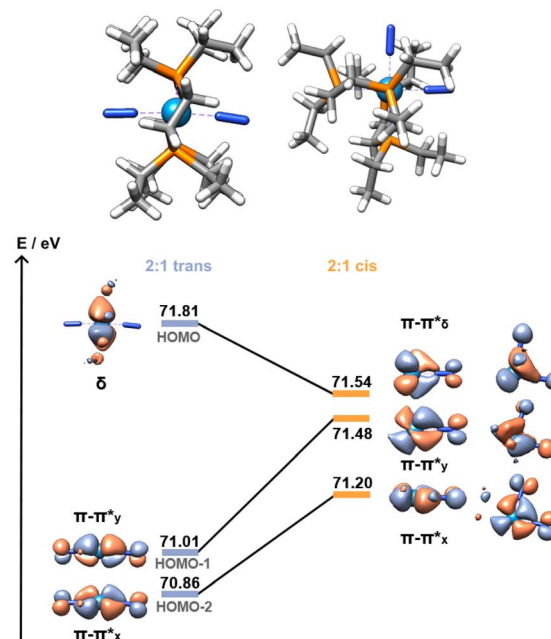
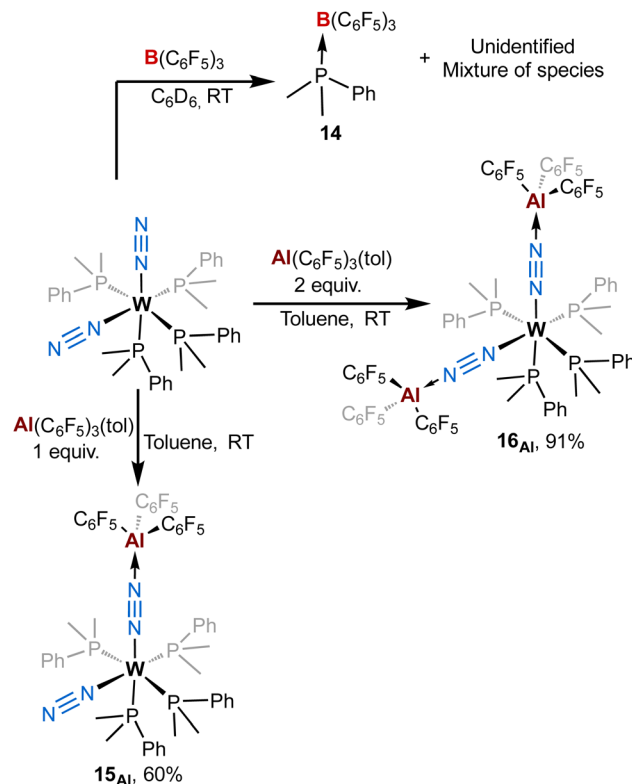


Fig. 7 *Cis* (11Al) vs. *trans* (8Al) frontier orbitals (HOMO to HOMO-2). **AlCF** omitted for clarity. Orbitals of the *cis* isomer are shown in side and top views.

a metal-centred orbital in the *trans* isomer – is significantly modified, forming an additional $\pi-\pi^*$ interaction in the *cis* isomer. This yields a total population of 6 electrons in N–N antibonding frontier orbitals instead of 4, leading to a greater overall activation of the N–N bond. The higher extent of the overlap between the metal and ligand orbitals is also likely responsible for the greater stability of this form.

Case of a monophosphine-supported W–N₂ complex

To get more insights about the divergent chemical behaviours of **AlCF** vs. **BCF** towards bis-dinitrogen complexes, we also investigated their reactivity with *cis*-[ML'₄(N₂)₂] species (M = Mo or W, L' = dimethylphenylphosphine). Stoichiometric treatment of **BCF** with *cis*-[WL'₄(N₂)₂] leads to the partial abstraction of one PMe₂Ph ligand to form a **BCF**-phosphine adduct – species **14** – (Scheme 4-top left) with a complex mixture of species (see ESI†) that we were not able to identify (except some remaining starting dinitrogen complex). From this experiment we concluded that adjunction of the Lewis acid mainly triggered decomposition. Furthermore, this highlights the ease for **BCF** to dissociate a monophosphine ligand suggesting its stronger affinity for PMe₂Ph vs. N₂. On the opposite, using similar conditions to that of the [M(depe)₂(N₂)₂] series, the reaction of **AlCF** with *cis*-[ML'₄(N₂)₂] (M = W) produces new LA-dinitrogen adducts – products **15_{Al}** and **16_{Al}** (Scheme 4, bottom). First clues about the identity of the mono adduct **15_{Al}** is evidenced by NMR spectroscopy. Indeed, its ³¹P NMR spectrum displays three signals at chemical shifts of -18.8, -22.1, and -25.5 ppm integrating respectively for 1, 2 and 1 phosphorus nuclei. This NMR signature suggests that **15_{Al}** is *cis*-[W(PMe₂Ph)₄(N₂)₂{μ-N₂-Al(C₆F₅)₃}] having one terminal dinitrogen motif and one



Scheme 4 Reactivity of $[M(PMe_2Ph)_4(N_2)_2]$ (M = W or Mo) complexes with (top) $B(C_6F_5)_3$ and (bottom) $Al(C_6F_5)_3(\text{tol})$.

bridging dinitrogen fragment. These above aspects are confirmed by IR spectroscopy where coordination of one $AlClF$ molecule at one distal nitrogen induces an averaged bathochromic shift of -171 cm^{-1} of the $\mu\text{-}N\equiv N$ IR band $-1776\text{ vs. }1947\text{ cm}^{-1}$ in *cis*- $[W(PMe_2Ph)_4(N_2)_2]$ — and an averaged hypsochromic shift of $+89\text{ cm}^{-1}$ of the terminal $N\equiv N$ stretching mode $-2037\text{ vs. }1947\text{ cm}^{-1}$ in *cis*- $[W(PMe_2Ph)_4(N_2)_2]$. Unfortunately, despite the good purity of 15_{Al} verified by elemental and spectroscopic analysis, our attempts to get single crystals were unsuccessful.

Addition of two equivalents of $Al(C_6F_5)_3(\text{tol})$ on *cis*- $[W(PMe_2Ph)_4(N_2)_2]$ produced a new two-fold adduct 16_{Al} —*cis*- $[W(PMe_2Ph)_4\{\mu\text{-}N_2\text{-}Al(C_6F_5)_3\}_2]$ — that was fully characterised in solution and in the solid-state. Spectroscopic and crystallographic data of 16_{Al} are very close to those of its congeners 11_{Al} (M = W), 12_{Al} (M = Mo), and 13_{Al} (M = Cr), showing a *cis* geometry for the $AlClF\text{-}(\mu\text{-}N_2)$ fragments (see Table 3). Indeed, aside from their ^{31}P NMR chemical shifts, the IR and XRD data of 16_{Al} vs. 11_{Al} are almost identical (see Table 3 and Fig. 8).

Electronic spectroscopy of the depe-supported W complexes

The recorded UV-vis absorption spectra of *trans*- $[M(\text{depe})_2(N_2)_2]$ (M = W and Mo) at 298 K display two types of bands, an intense transition ($320\text{-}330\text{ nm}$, $\epsilon \approx 10^5\text{ M}^{-1}\text{ cm}^{-1}$) assigned to metal-to-ligand charge transfer (MLCT) involving a ligand phosphorus atom, and a less intense transition ($440\text{-}500\text{ nm}$, $\epsilon \approx 10^3\text{ M}^{-1}\text{ cm}^{-1}$) assigned to a ligand field (LF) d-d transition.⁸⁵

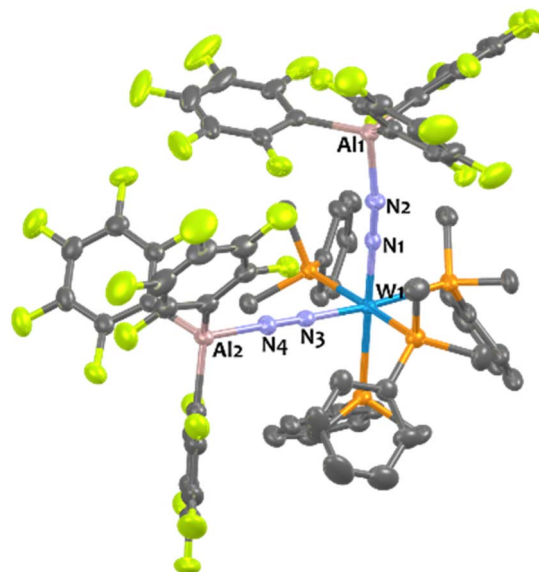


Fig. 8 Solid-state structure of 16_{Al} . Ellipsoids are represented with 30% probability. Hydrogen atoms have been omitted for clarity. Selected bond distances (Å) and angles (°): $Al_1\text{-}N_2$ 1.915(3), $Al_2\text{-}N_4$ 1.891(3), $W_1\text{-}N_1$ 1.917(3), $W_1\text{-}N_3$ 1.906(3), $N_1\text{-}N_2$ 1.149(4), $N_3\text{-}N_4$ 1.150(4), $W_1\text{-}N_1\text{-}N_2$ 179.2(3), $W_1\text{-}N_3\text{-}N_4$ 177.5(3), $N_1\text{-}W_1\text{-}N_3$ 91.34(1), $Al_1\text{-}N_2\text{-}N_1$ 168.5(3), $Al_2\text{-}N_4\text{-}N_3$ 179.1(3).

The MLCT transition of the aluminium and boron adducts does not shift substantially ($\Delta\lambda < 3\text{ nm}$) compared to that of the W starting complex (Fig. 9). However, their intensities are about two times lower compared to the W starting complex. We thus assign these energetically similar UV signatures to the

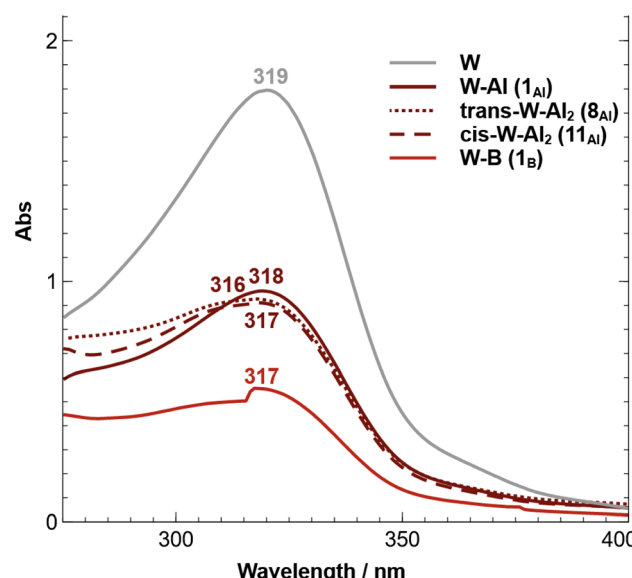


Fig. 9 Absorption spectra of *trans*- $[W(\text{depe})_2(N_2)_2]$ (W , grey line), *trans*- $[W(\text{depe})_2(\mu\text{-}N_2\text{-}Al(C_6F_5)_3)]$ ($W\text{-}Al$, crimson line), *trans*- $[W(\text{depe})_2\{\mu\text{-}N_2\text{-}Al(C_6F_5)_3\}_2]$ (*trans*- $W\text{-}Al_2$, dotted crimson line), *cis*- $[W(\text{depe})_2\{\mu\text{-}N_2\text{-}Al(C_6F_5)_3\}_2]$ (*cis*- $W\text{-}Al_2$, dashed crimson line), and *trans*- $[W(\text{depe})_2(N_2)(\mu\text{-}N_2\text{-}B(C_6F_5)_3)]$ ($W\text{-}B$, red line). The concentration of each sample is about 30 μM .



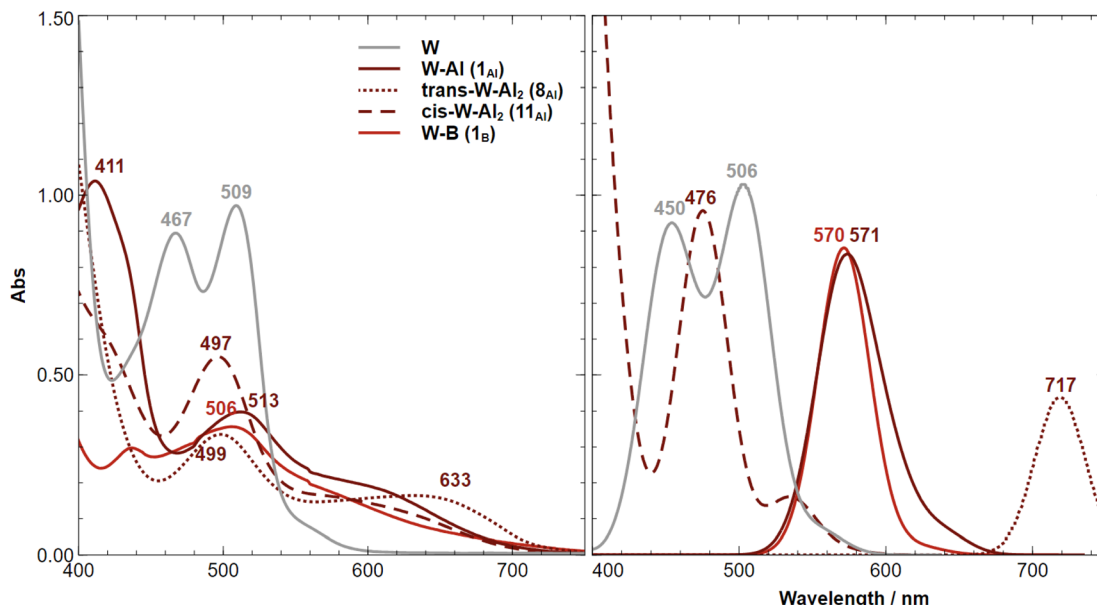


Fig. 10 Experimental (left) and computational (CAM-B3LYP, right) absorption spectra of $trans$ -[W(depe)₂(N₂)₂] (W, grey line), $trans$ -[W(depe)₂(N₂)₂Al(C₆F₅)₃] (W-Al, crimson line), $trans$ -[W(depe)₂(μ -N₂-Al(C₆F₅)₃)₂] (trans-W-Al₂, dotted crimson line), cis -[W(depe)₂(μ -N₂-Al(C₆F₅)₃)₂] (cis-W-Al₂, dashed crimson line), and $trans$ -[W(depe)₂(N₂)₂(μ -N₂-B(C₆F₅)₃)] (W-B, red line). The concentration of each sample is about 1000 μ M. A Lorentzian line broadening with FWHM of 8 was applied to the computed peaks.

chemical environment around the W-P that does not change substantially upon coordination of the LA (unlike the dinitrogen ligand where the coordination of **AlCF** or **BCF** takes place). Fig. 10 (left side) displays the visible spectra of each sample at a concentration of 10^{-3} M. The $trans$ -W(depe)₂(N₂)₂ starting complex displayed two LF (d-d transitions) bands at $\lambda_1 = 467$ nm and $\lambda_2 = 509$ nm in agreement with literature data.⁸⁵ For the Al mono adduct (W-Al, crimson line) we observed a significant blue shift of the first band — $\lambda_1 = 411$ nm— and a small red shift of the second band — $\lambda_2 = 513$ nm. For the boron mono-adduct (red line), we observed a slight blue shift for the first and second bands ($\lambda_1 = 437$ nm, $\lambda_2 = 506$ nm). The Al double adducts of $trans$ configuration display two new bands (crimson dotted line), one at a wavenumber of 499 nm and the other at a high wavenumber of 633 nm (this complex has a green-cyan colour). For the *cis*-double adduct, the spectrum displays a single maximum in the visible region at 497 nm. Note that for all the Al and B adducts, we noticed absorption in the [550–700 nm] spectral window (unlike the W starting complex where there is no absorption at all in this area).

Computing the electronic excitation spectra of transition-metal complexes with a high degree of quantitative accuracy is far from trivial.⁸⁶ Nevertheless TD-DFT calculations are key to provide understanding into the nature of the transitions responsible for the UV-vis bands. The peaks obtained *via* TD-DFT calculations (CAM-B3LYP/def2-TZVP) are in qualitative agreement with the recorded spectra, albeit being generally red shifted by *ca.* 30–60 nm, except for the bare tungsten complex in which an almost exact match is obtained. The mono-substituted adducts have almost overlapping spectra in both experiment and computations. Two peaks are observed in the

experimental UV spectrum of **11_{Al}** (*trans*-W-Al₂, Fig. 10-left) while the computed one displays just one. A second, considerably red-shifted peak is visible in the computed spectrum at wavelengths greater than 750 nm (Fig. S97†). An analysis of the Natural Transition Orbitals (NTOs) shows, however, that these do not correspond to d-d transitions, but instead to low-lying MLCT transitions from the metal to both nitrogen ligands (Fig. 11). Such low-lying charge transfer transitions had already

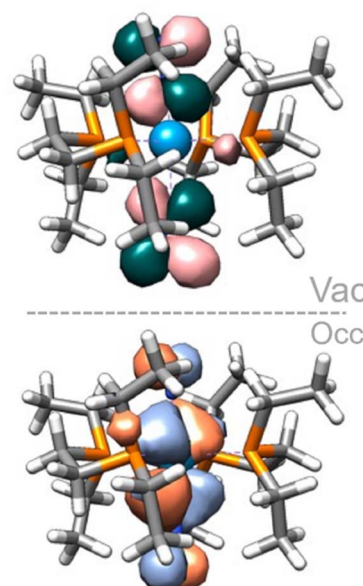


Fig. 11 NTOs (occupied – bottom, vacant – top) of the 450 nm band of the bare tungsten complex.



been identified in a Ru(II) complex⁸⁷ that has, like the compounds studied here, a ligand-based LUMO orbital. Remaining relevant NTOs as well as the calculated peaks and associated difference densities can be found in Fig. S94–S96.[†]

Conclusions

This work was motivated by previous results from our groups having thoroughly investigated, experimentally on the one hand, the coordination of tris(pentafluorophenyl)borane, **BCF**, to formally zerovalent group 6 bis(dinitrogen) complexes supported with phosphine ligands, and computationally on the other hand, the influence of LA binding to a dinitrogen ligand. This combined experimental/theoretical study explores similar chemistry employing tris(pentafluorophenyl)alane, **AlCF**. The shift to a structurally comparable but more Lewis acidic species led to the isolation of related 1 : 1 adducts of an extensive family of dinitrogen complexes, including a chromium-based and monophosphine-based ones that could not be selectively formed when **BCF** was employed. A notable difference on the structural point of view is the linear N–N–Al *vs.* bent N–N–B motif that is explained by steric repulsion between the C₆F₅ groups with the ethyl substituents of the phosphines built up as a result of longer Al–C bonds.

Unlike **BCF**, **AlCF** makes robust two-fold μ -N₂ adducts with the *bis*(dinitrogen) complexes. They form with an initial *trans* arrangement that evolves in solution to a more stable *cis* one with a rate depending on the metal (Cr > Mo > W). To the best of our knowledge, these compounds are the first examples of tri-nuclear heterobimetallic complexes formed by Lewis acid–base interaction exhibiting p and d elements. Among the handful of N₂-bridged tri-nuclear heterobimetallic species^{88–98} of general formula M₁(μ -N₂)M₂(μ -N₂)M₁ (M₁ = Cr,⁸⁹ Mo,^{95–97} Re,⁹² Fe,⁹³ Co,^{90,91,93,94,98} M₂ = Na,⁹⁵ Mg,^{90,91,93–95,97,98} Ti,⁸⁹ Zr,^{92,96} V,⁹⁶ Fe⁹⁶), many are based on a low diversity of metal/metal couples, typically on magnesium/early transition metals pairs, as a result of a formally anionic dinitrogen complex formed by reduction with an alkaline or alkaline-earth metal. For the synthesis of d-block-only congeners, a general strategy consists in halide substitution by an electron-rich N₂ ligand, a transformation that accompanies with formal oxidation of the N₂-ligated metal centre concomitant with reduction of N₂. Here, the novelty of our $\text{bis}(\mu\text{-}\eta^1\text{:}\eta^1\text{-N}_2\text{-AlCF})$ specimens resides in the use of a p-block metal that interacts with neutral group 6 N₂ complexes through Lewis acid–base pair formation, through straightforward syntheses (no redox state change, no by-products, and no workup). Note that this synthetic approach parallels a recent work published by Mazzanti and coworkers where they reported the coordination of f-elements (lanthanides and uranium) to an end-on dinitrogen iron complex leading to the formation of N₂ bridged heterobimetallic adducts.⁹⁹ Last but not least, the close proximity of the two activated dinitrogen motifs in these adducts (imparted by their *cis*-configuration) may pave the way towards new type of N₂ reactivity. DFT calculations show that the diminished level of N₂ activation in these systems, evidenced experimentally by comparison of IR and XRD data to those of the 1 : 1 adducts, can be interpreted by a destabilisation

of a σ -symmetric, W–N antibonding component of the W–N–N bonding. While the “bare” N₂ complexes, their 1 : 1 and *trans*-2:1 Lewis acid adducts have a HOMO of pure d character, in the *cis*-2:1 adducts this orbital overlaps with a π^* orbital of each N₂ ligands. This could result, in terms of reactivity, into a selective reactivity of the N₂ ligands towards electrophiles *vs.* the metal centre. From the bare [W(depe)₂(N₂)₂] complex to the two-fold aluminium adduct, substantial decrease of the HOMO–LUMO gap is noticed. In particular, the stabilized N₂-centered LUMO should more easily accept electrons, suggesting Lewis acids could be co-activators for (electro) catalysed N₂ reduction.

Electronic spectroscopy was examined for the depe-supported W–N₂ complex and its adducts both experimentally and computationally. This investigation suggests that the nature of the observed absorptions in the visible spectrum is an unusual low-lying MLCT involving N₂-centered orbitals that significantly red-shifts upon LA coordination. This could have important implication for visible light-driven nitrogen fixation, and we are currently exploring the reactivity of LA-adducts of N₂ complexes towards this end.

Data availability

The datasets supporting this article have been uploaded as part of the ESI.[†] All the computational data have been uploaded (<https://www.iochem-bd.org/handle/10/229000>) onto the ioChem-BD platform (<https://www.iochem-bd.org/>) to facilitate data exchange and dissemination, according to the FAIR principles of OpenData sharing.

Author contributions

Conceptualization: A. S.; formal analysis: L. E., L. V., A. C., N. Q.; funding acquisition: A. S., V. K.; investigation L. E., A. C., N. Q., F. M.; methodology: L. E., A. C., N. Q., F. M., V. K., A. S.; project administration: V. K., A. S.; supervision V. K., A. S.; validation: L. E., F. M.; visualization: L. E., F. M.; writing – original draft: L. E., F. M.; writing – review & editing: V. K., A. S.

Conflicts of interest

There are no conflicts to declare.

Acknowledgements

L. E. and A. S. thanks the French Agence Nationale de la Recherche for funding (grant ANR-21-CE07-0003). N. Q. and A. S. are indebted to the European Research Council for funding (ERC Starting Grant no 757501). A. C. is grateful to the French Ministry of National and Superior Education and Research (MENESR) for a PhD fellowship. F. F. M. gratefully acknowledges a Career Bridging Grant from TU Darmstadt. We are grateful to the CNRS (Centre National de la Recherche Scientifique) and the Technische Universität Darmstadt for providing access to facilities, specifically the Lichtenberg II high performance computer at TU Darmstadt on which all calculations for this work were performed.



Notes and references

1 A. D. Allen and C. V. Senoff, Nitrogenopentamineruthenium(II) complexes, *Chem. Commun.*, 1965, 621.

2 M. J. Chalkley, M. W. Dровер and J. C. Peters, Catalytic N₂-to-NH₃ (or -N₂H₄) Conversion by Well-Defined Molecular Coordination Complexes, *Chem. Rev.*, 2020, **120**, 5582–5636.

3 Y. Roux, C. Duboc and M. Gennari, Molecular Catalysts for N₂ Reduction: State of the Art, Mechanism, and Challenges, *ChemPhysChem*, 2017, **18**, 2606–2617.

4 M. Pérez-Jiménez, H. Corona, F. de la Cruz-Martínez and J. Campos, Donor–Acceptor Activation of Carbon Dioxide, *Chem.–Eur. J.*, 2023, **29**, e202301428.

5 D. W. Stephan and G. Erker, Frustrated Lewis pair chemistry of carbon, nitrogen and sulfur oxides, *Chem. Sci.*, 2014, **5**, 2625–2641.

6 A. E. Ashley and D. O'Hare, FLP-Mediated Activations and Reductions of CO₂ and CO, *Top. Curr. Chem.*, 2013, **334**, 191–217.

7 R. M. Bullock and G. M. Chambers, Frustration across the periodic table: heterolytic cleavage of dihydrogen by metal complexes, *Philos. Trans. R. Soc., A*, 2017, **375**, 20170002.

8 D. W. Stephan, Diverse Uses of the Reaction of Frustrated Lewis Pair (FLP) with Hydrogen, *J. Am. Chem. Soc.*, 2021, **143**, 20002–20014.

9 M. A. Stevens and A. L. Colebatch, Cooperative approaches in catalytic hydrogenation and dehydrogenation, *Chem. Soc. Rev.*, 2022, **51**, 1881–1898.

10 J. C. Slootweg and A. R. Jupp, *Frustrated Lewis Pairs*, Springer Nature, 2020.

11 F.-G. Fontaine and D. W. Stephan, On the concept of frustrated Lewis pairs, *Philos. Trans. R. Soc., A*, 2017, **375**, 20170004.

12 D. W. Stephan, The broadening reach of frustrated Lewis pair chemistry, *Science*, 2016, **354**, aaf7229.

13 D. W. Stephan, Frustrated Lewis Pairs: From Concept to Catalysis, *Acc. Chem. Res.*, 2015, **48**, 306–316.

14 D. W. Stephan and G. Erker, Frustrated Lewis Pair Chemistry: Development and Perspectives, *Angew. Chem., Int. Ed.*, 2015, **54**, 6400–6441.

15 *Frustrated Lewis Pairs II: Expanding the Scope*, ed. G. Erker and D. W. Stephan, Springer Berlin Heidelberg, 2013.

16 *Frustrated Lewis Pairs I: Uncovering and Understanding*, ed. G. Erker and D. W. Stephan, Springer Berlin Heidelberg, 2013.

17 D. W. Stephan and G. Erker, Frustrated Lewis Pairs: Metal-free Hydrogen Activation and More, *Angew. Chem., Int. Ed.*, 2010, **49**, 46–76.

18 B. Chatterjee, W.-C. Chang, S. Jena and C. Werlé, Implementation of Cooperative Designs in Polarized Transition Metal Systems—Significance for Bond Activation and Catalysis, *ACS Catal.*, 2020, **10**, 14024–14055.

19 E. R. M. Habraken, A. R. Jupp, M. B. Brands, M. Nieger, A. W. Ehlers and J. C. Slootweg, Parallels between Metal-Ligand Cooperativity and Frustrated Lewis Pairs, *Eur. J. Inorg. Chem.*, 2019, **2019**, 2436–2442.

20 P. C. Dos Santos, R. Y. Igarashi, H.-I. Lee, B. M. Hoffman, L. C. Seefeldt and D. R. Dean, Substrate Interactions with the Nitrogenase Active Site, *Acc. Chem. Res.*, 2005, **38**, 208–214.

21 T. Spatzal, K. A. Perez, O. Einsle, J. B. Howard and D. C. Rees, Ligand binding to the FeMo-cofactor: Structures of CO-bound and reactivated nitrogenase, *Science*, 2014, **345**, 1620–1623.

22 S. M. Keable, J. Vertemara, O. A. Zadvornyy, B. J. Eilers, K. Danyal, A. J. Rasmussen, L. De Gioia, G. Zampella, L. C. Seefeldt and J. W. Peters, Structural characterization of the nitrogenase molybdenum-iron protein with the substrate acetylene trapped near the active site, *J. Inorg. Biochem.*, 2018, **180**, 129–134.

23 D. Sippel, M. Rohde, J. Netzer, C. Trncik, J. Gies, K. Grunau, I. Djurdjevic, L. Decamps, S. L. A. Andrade and O. Einsle, A bound reaction intermediate sheds light on the mechanism of nitrogenase, *Science*, 2018, **359**, 1484–1489.

24 W. Kang, C. C. Lee, A. J. Jasniewski, M. W. Ribbe and Y. Hu, Structural evidence for a dynamic metallocofactor during N₂ reduction by Mo-nitrogenase, *Science*, 2020, **368**, 1381–1385.

25 J. B. Geri, J. P. Shanahan and N. K. Szymczak, Testing the Push–Pull Hypothesis: Lewis Acid Augmented N₂ Activation at Iron, *J. Am. Chem. Soc.*, 2017, **139**, 5952–5956.

26 J. P. Shanahan and N. K. Szymczak, Hydrogen Bonding to a Dinitrogen Complex at Room Temperature: Impacts on N₂ Activation, *J. Am. Chem. Soc.*, 2019, **141**, 8550–8556.

27 J. J. Mortensen, B. Hammer and J. K. Nørskov, Alkali Promotion of N₂ Dissociation over Ru(0001), *Phys. Rev. Lett.*, 1998, **80**, 4333–4336.

28 S. Dahl, A. Logadottir, C. J. H. Jacobsen and J. K. Nørskov, Electronic factors in catalysis: the volcano curve and the effect of promotion in catalytic ammonia synthesis, *Appl. Catal., A*, 2001, **222**, 19–29.

29 G. P. Connor and P. L. Holland, Coordination chemistry insights into the role of alkali metal promoters in dinitrogen reduction, *Catal. Today*, 2017, **286**, 21–40.

30 Q. Wang, J. Guo and P. Chen, The impact of alkali and alkaline earth metals on green ammonia synthesis, *Chem.*, 2021, **7**, 3203–3220.

31 A. Coffinet, A. Simonneau and D. Specklin, in *Encyclopedia of Inorganic and Bioinorganic Chemistry*, ed. R. A. Scott, Wiley, 2nd edn, 2020, pp. 1–25.

32 A. J. Ruddy, D. M. C. Ould, P. D. Newman and R. L. Melen, Push and pull: the potential role of boron in N₂ activation, *Dalton Trans.*, 2018, **47**, 10377–10381.

33 A. Simonneau and M. Etienne, Enhanced Activation of Coordinated Dinitrogen with p-Block Lewis Acids, *Chem. – Eur. J.*, 2018, **24**, 12458–12463.

34 J. Chatt, J. R. Dilworth, R. L. Richards and J. R. Sanders, Chemical Evidence concerning the Function of Molybdenum in Nitrogenase, *Nature*, 1969, **224**, 1201–1202.

35 J. Chatt, R. H. Crabtree and R. L. Richards, Dinitrogen- and carbonyl-complexes as bases towards trimethylaluminium, *J. Chem. Soc. Chem. Commun.*, 1972, 534.

36 J. Chatt, R. H. Crabtree, E. A. Jeffery and R. L. Richards, The basic strengths of some dinitrogen complexes of



molybdenum(0), tungsten(0), rhenium(I), and osmium(II), *J. Chem. Soc., Dalton Trans.*, 1973, 1167–1172.

37 F. Studt, B. A. MacKay, S. A. Johnson, B. O. Patrick, M. D. Fryzuk and F. Tuczek, Lewis adducts of the side-on end-on dinitrogen-bridged complex $[(\text{NPN})\text{Ta}_2(\mu\text{-H})_2(\mu\text{-}\eta^1\text{:}\eta^2\text{-N}_2)]$ with AlMe_3 , GaMe_3 , and $\text{B}(\text{C}_6\text{F}_5)_3$: Synthesis, structure, and spectroscopic properties, *Chem.-Eur. J.*, 2005, **11**, 604–618.

38 H. Broda, S. Hinrichsen, J. Krahmer, C. Nather and F. Tuczek, Molybdenum dinitrogen complexes supported by a silicon-centred tripod ligand and dppm or dmpm: tuning the activation of N_2 , *Dalton Trans.*, 2014, **43**, 2007–2012.

39 A. Simonneau, R. Turrel, L. Vendier and M. Etienne, Group 6 Transition-Metal/Boron Frustrated Lewis Pair Templates Activate N_2 and Allow its Facile Borylation and Silylation, *Angew. Chem., Int. Ed.*, 2017, **56**, 12268–12272.

40 D. Specklin, M.-C. Boegli, A. Coffinet, L. Escomel, L. Vendier, M. Grellier and A. Simonneau, An orbitally adapted push-pull template for N_2 activation and reduction to diazene-diide, *Chem. Sci.*, 2023, **14**, 14262–14270.

41 A. D. Piascik, P. J. Hill, A. D. Crawford, L. R. Doyle, J. C. Green and A. E. Ashley, Cationic silyldiazenido complexes of the $\text{Fe}(\text{diphosphine})_2(\text{N}_2)$ platform: structural and electronic models for an elusive first intermediate in N_2 fixation, *Chem. Commun.*, 2017, **53**, 7657–7660.

42 L. G. Pap, A. Couldridge, N. Arulسامي and E. Hulley, Electrostatic polarization of nonpolar substrates: a study of interactions between simple cations and Mo-bound N_2 , *Dalton Trans.*, 2019, **48**, 11004–11017.

43 D. Specklin, A. Coffinet, L. Vendier, I. del Rosal, C. Dinoi and A. Simonneau, Synthesis, Characterization, and Comparative Theoretical Investigation of Dinitrogen-Bridged Group 6-Gold Heterobimetallic Complexes, *Inorg. Chem.*, 2021, **60**, 5545–5562.

44 C. Tang, Q. Liang, A. R. Jupp, T. C. Johnstone, R. C. Neu, D. Song, S. Grimme and D. W. Stephan, 1,1-Hydroboration and a Borane Adduct of Diphenyldiazomethane: A Potential Prelude to FLP- N_2 Chemistry, *Angew. Chem., Int. Ed.*, 2017, **56**, 16588–16592.

45 F. F. Martins and V. Krewald, Cooperative Dinitrogen Activation: Identifying the Push–Pull Effects of Transition Metals and Lewis Acids in Molecular Orbital Diagrams, *Eur. J. Inorg. Chem.*, 2023, **26**, e202300268.

46 L. Greb, Lewis Superacids: Classifications, Candidates, and Applications, *Chem.-Eur. J.*, 2018, **24**, 17881–17896.

47 J. L. W. Pohlmann and F. E. Brinckmann, Preparation and Characterization of Group III A Derivatives, *Z. Naturforsch. B*, 1965, **20**, 5–11.

48 T. Belgardt, J. Storre, H. W. Roesky, M. Noltemeyer and H.-G. Schmidt, Tris(pentafluorophenyl)alane: A Novel Aluminum Organyl, *Inorg. Chem.*, 1995, **34**, 3821–3822.

49 G. S. Hair, A. H. Cowley, R. A. Jones, B. G. McBurnett and A. Voigt, Arene Complexes of $\text{Al}(\text{C}_6\text{F}_5)_3$. Relationship to a Déjà Vu Silylum Ion, *J. Am. Chem. Soc.*, 1999, **121**, 4922–4923.

50 J. Klosin, G. R. Roof, E. Y.-X. Chen and K. A. Abboud, Ligand Exchange and Alkyl Abstraction Involving (Perfluoroaryl) boranes and -alanes with Aluminum and Gallium Alkyls, *Organometallics*, 2000, **19**, 4684–4686.

51 S. Feng, G. R. Roof and E. Y.-X. Chen, Tantalum(V)-Based Metallocene, Half-Metallocene, and Non-Metallocene Complexes as Ethylene–1-Octene Copolymerization and Methyl Methacrylate Polymerization Catalysts, *Organometallics*, 2002, **21**, 832–839.

52 N. G. Stahl, M. R. Salata and T. J. Marks, $\text{B}(\text{C}_6\text{F}_5)_3$ vs $\text{Al}(\text{C}_6\text{F}_5)_3$ -Derived Metallocenium Ion Pairs. Structural, Thermochemical, and Structural Dynamic Divergences, *J. Am. Chem. Soc.*, 2005, **127**, 10898–10909.

53 J. Chen and E. Y.-X. Chen, Unsolvated $\text{Al}(\text{C}_6\text{F}_5)_3$: structural features and electronic interaction with ferrocene, *Dalton Trans.*, 2016, **45**, 6105–6110.

54 D. M. C. Ould, J. L. Carden, R. Page and R. L. Melen, Synthesis and Reactivity of Fluorinated Triaryl Aluminum Complexes, *Inorg. Chem.*, 2020, **59**, 14891–14898.

55 I. V. Kazakov, A. S. Lisovenko, N. A. Shcherbina, I. V. Korniyakov, N. Y. Gugin, Y. V. Kondrat'ev, A. M. Chernysheva, A. S. Zavgorodnii and A. Y. Timoshkin, Structural and Energetic Features of Group 13 Element Tris(pentafluorophenyl) Complexes with Diethyl Ether, *Eur. J. Inorg. Chem.*, 2020, **2020**, 4442–4449.

56 A. Y. Timoshkin, The Field of Main Group Lewis Acids and Lewis Superacids: Important Basics and Recent Developments, *Chem.-Eur. J.*, 2024, **30**, e202302457.

57 L. Pauling, Atomic Radii and Interatomic Distances in Metals, *J. Am. Chem. Soc.*, 1947, **69**, 542–553.

58 W. E. Piers and T. Chivers, Pentafluorophenylboranes: from obscurity to applications, *Chem. Soc. Rev.*, 1997, **26**, 345.

59 J. R. Lawson and R. L. Melen, Tris(pentafluorophenyl)borane and Beyond: Modern Advances in Borylation Chemistry, *Inorg. Chem.*, 2017, **56**, 8627–8643.

60 J. Chen and E. Y.-X. Chen, Elusive Silane–Alane Complex $[\text{SiH}\cdots\text{Al}]$: Isolation, Characterization, and Multifaceted Frustrated Lewis Pair Type Catalysis, *Angew. Chem., Int. Ed.*, 2015, **54**, 6842–6846.

61 K. O. Christe, D. A. Dixon, D. McLemore, W. W. Wilson, J. A. Sheehy and J. A. Boatz, On a quantitative scale for Lewis acidity and recent progress in polynitrogen chemistry, *J. Fluorine Chem.*, 2000, **101**, 151–153.

62 J. C. Haartz and D. H. McDaniel, Fluoride ion affinity of some Lewis acids, *J. Am. Chem. Soc.*, 1973, **95**, 8562–8565.

63 E. Y.-X. Chen, W. J. Kruper, G. Roof and D. R. Wilson, Double Activation of Constrained Geometry and *ansa*-Metallocene Group 4 Metal Dialkyls: Synthesis, Structure, and Olefin Polymerization Study of Mono- and Dicationic Aluminate Complexes, *J. Am. Chem. Soc.*, 2001, **123**, 745–746.

64 A. Y. Timoshkin and G. Frenking, Gas-Phase Lewis Acidity of Perfluoroaryl Derivatives of Group 13 Elements, *Organometallics*, 2008, **27**, 371–380.

65 J. F. Kögel, D. A. Sorokin, A. Khvorost, M. Scott, K. Harms, D. Himmel, I. Krossing and J. Sundermeyer, The Lewis superacid $\text{Al}[\text{N}(\text{C}_6\text{F}_5)_2]_3$ and its higher homolog $\text{Ga}[\text{N}(\text{C}_6\text{F}_5)_2]_3$ – structural features, theoretical investigation



and reactions of a metal amide with higher fluoride ion affinity than SbF_5 , *Chem. Sci.*, 2017, **9**, 245–253.

66 T. A. George and M. E. Noble, A direct one-step preparation of bis(dinitrogen) complexes of molybdenum(0) from molybdenum(V) chloride, *Inorg. Chem.*, 1978, **17**, 1678–1679.

67 J. R. Dilworth, R. L. Richards, G. J.-J. Chen and J. W. McDonald, in *Inorganic Syntheses*, John Wiley & Sons, Ltd, 1990, pp. 33–43.

68 R. Poli and H. D. Mui, True nature of trihalotris(tetrahydrofuran)molybdenum(III), $\text{MoX}_3(\text{THF})_3$ ($\text{X} = \text{Cl}, \text{Br}, \text{I}$). A paramagnetic proton NMR study, *J. Am. Chem. Soc.*, 1990, **112**, 2446–2448.

69 F. Stoffelbach, D. Saurenz and R. Poli, Improved Preparations of Molybdenum Coordination Compounds from Tetrachlorobis(diethyl ether)molybdenum(IV), *Eur. J. Inorg. Chem.*, 2001, 2699–2703.

70 A. C. Filippou, G. Schnakenburg, A. I. Philippopoulos and N. Weidemann, Ge_2 trapped by triple bonds between two metal centers: the germylidyne complexes *trans,trans*- $[\text{Cl}(\text{depe})_2\text{M}\equiv\text{Ge}—\text{Ge}\equiv\text{M}(\text{depe})_2\text{Cl}]$ ($\text{M}=\text{Mo}, \text{W}$) and bonding analyses of the $\text{M}\equiv\text{Ge}—\text{Ge}\equiv\text{M}$ chain, *Angew. Chem., Int. Ed.*, 2005, **44**, 5979–5985.

71 E. M. Zolnhofer, A. A. Opalade, T. A. Jackson, F. W. Heinemann, K. Meyer, J. Krzystek, A. Ozarowski and J. Telser, Electronic Structure and Magnetic Properties of a Low-Spin Cr^{II} Complex: *trans*- $[\text{CrCl}_2(\text{dmpe})_2]$ ($\text{dmpe} = 1,2\text{-Bis(dimethylphosphino)ethane}$), *Inorg. Chem.*, 2021, **60**, 17865–17877.

72 G. S. Girolami, G. Wilkinson, A. M. R. Galas, M. Thornton-Pett and M. B. Hursthouse, Synthesis and properties of the divalent 1,2-bis(dimethylphosphino)ethane (dmpe) complexes $\text{MCl}_2(\text{dmpe})_2$ and $\text{MMe}_2(\text{dmpe})_2$ ($\text{M} = \text{Ti}, \text{V}, \text{Cr}, \text{Mn}, \text{or Fe}$). X-Ray crystal structures of $\text{MCl}_2(\text{dmpe})_2$ ($\text{M} = \text{Ti}, \text{V}, \text{or Cr}$), $\text{MnBr}_2(\text{dmpe})_2$, $\text{TiMe}_{1.3}\text{Cl}_{0.7}(\text{dmpe})_2$, and $\text{CrMe}_2(\text{dmpe})_2$, *J. Chem. Soc., Dalton Trans.*, 1985, 1339.

73 A. J. Kendall, S. I. Johnson, R. M. Bullock and M. T. Mock, Catalytic Silylation of N_2 and Synthesis of NH_3 and N_2H_4 by Net Hydrogen Atom Transfer Reactions Using a Chromium P_4 Macrocycle, *J. Am. Chem. Soc.*, 2018, **140**, 2528–2536.

74 J. E. Salt, G. S. Girolami, G. Wilkinson, M. Motevalli, M. Thornton-Pett and M. B. Hursthouse, Synthesis and characterisation of 1,2-bis(dimethylphosphino)ethane (dmpe) complexes of chromium-(0) and -(IV): X-ray crystal structures of *trans*- $\text{Cr}(\text{N}_2)_2(\text{dmpe})_2$, *cis*- $\text{Cr}(\text{CO})_2(\text{dmpe})_2$, $\text{Cr}(\text{C}_2\text{Ph}_2)_2(\text{dmpe})$, and $\text{CrH}_4(\text{dmpe})_2$, *J. Chem. Soc., Dalton Trans.*, 1985, 685.

75 L. A. Berben and S. A. Kozimor, Dinitrogen and Acetylidyne Complexes of Low-Valent Chromium, *Inorg. Chem.*, 2008, **47**, 4639–4647.

76 J. He, Y. Zhang, L. Falivene, L. Caporaso, L. Cavallo and E. Y.-X. Chen, Chain Propagation and Termination Mechanisms for Polymerization of Conjugated Polar Alkenes by [Al]-Based Frustrated Lewis Pairs, *Macromolecules*, 2014, **47**, 7765–7774.

77 L. L. Cao, J. Zhou, Z. Qu and D. W. Stephan, Single Electron Transfer to Diazomethane–Borane Adducts Prompts C–H Bond Activations, *Angew. Chem., Int. Ed.*, 2019, **58**, 18487–18491.

78 T. Asada, Y. Hoshimoto and S. Ogoshi, Rotation-Triggered Transmetalation on a Heterobimetallic Cu/Al N-Phosphine-Oxide-Substituted Imidazolylidene Complex, *J. Am. Chem. Soc.*, 2020, **142**, 9772–9784.

79 Z. Yu, M. J. Heeg and C. H. Winter, A bridging ethyl complex of aluminium, *Chem. Commun.*, 2001, 353–354.

80 W. Uhl and F. Hannemann, A methylene bridged dialuminium compound as a chelating Lewis acid–complexation of azide and acetate anions by $\text{R}_2\text{Al}-\text{CH}_2-\text{AlR}_2$ [$\text{R}=\text{CH}(\text{SiMe}_3)_2$], *J. Organomet. Chem.*, 1999, **579**, 18–23.

81 J. Liu, T.-L. Lam, M.-K. Sit, Q. Wan, C. Yang, G. Cheng and C.-M. Che, Pure blue phosphorescent platinum(II) emitters supported by NHC-based pincer type ligands with unitary emission quantum yields, *J. Mater. Chem. C*, 2022, **10**, 10271–10283.

82 T. Voss, T. Mahdi, E. Otten, R. Fröhlich, G. Kehr, D. W. Stephan and G. Erker, Frustrated Lewis Pair Behavior of Intermolecular Amine/B(C_6F_5)₃ Pairs, *Organometallics*, 2012, **31**, 2367–2378.

83 K. Bläsing, J. Bresien, R. Labbow, D. Michalik, A. Schulz, M. Thomas and A. Villinger, Borane Adducts of Hydrazoic Acid and Organic Azides: Intermediates for the Formation of Aminoboranes, *Angew. Chem., Int. Ed.*, 2019, **58**, 6540–6544.

84 W. Uhl, F. Hannemann, W. Saak and R. Wartchow, Diazomethane Derivatives Bearing Dialkylaluminium or DialkylgalliumSubstituents – The Isomeric Diazomethane and Nitrile Imine Structures Realized by the Different Coordination Behavior of Aluminium and Gallium, *Eur. J. Inorg. Chem.*, 1999, **1999**, 771–776.

85 B. L. Nordwig, D. J. Ohlsen, K. D. Beyer, A. S. Wruck and J. G. Brummer, The Effect of the Diphosphine Basicity on the Excited-State Properties of *trans*- $(\text{N}_2)_2\text{W}(\text{R}_2\text{PCH}_2\text{CH}_2\text{PR}_2)_2$: Identification of Near-Degenerate, Luminescent $^3\text{MLCT}$ and ^3LF Terms, *Inorg. Chem.*, 2006, **45**, 858–867.

86 F. Maschietto, M. Campetella, J. Sanz García, C. Adamo and I. Ciofini, Chasing unphysical TD-DFT excited states in transition metal complexes with a simple diagnostic tool, *J. Chem. Phys.*, 2021, **154**, 204102.

87 Y. Sun, S. N. Collins, L. E. Joyce and C. Turro, Unusual Photophysical Properties of a Ruthenium(II) Complex Related to $[\text{Ru}(\text{bpy})_2(\text{dppz})]^{2+}$, *Inorg. Chem.*, 2010, **49**, 4257–4262.

88 T. Knoell, J. Polanco, S. N. MacMillan, J. A. Bertke, C. Foroutan-Nejad, K. M. Lancaster and A. Gus Bakhoda, Alkaline earth metal-assisted dinitrogen activation at nickel, *Dalton Trans.*, 2024, **53**, 4689–4697.

89 X. Wang, Y. Wang, Y. Wu, G.-X. Wang, J. Wei and Z. Xi, Syntheses and Characterizations of Hetero-Bimetallic Chromium-Dinitrogen Transition-Metal Complexes, *Inorg. Chem.*, 2023, **62**, 18641–18648.

90 B. A. Suslick and T. D. Tilley, Mechanistic Interrogation of Alkyne Hydroarylations Catalyzed by Highly Reduced,



Single-Component Cobalt Complexes, *J. Am. Chem. Soc.*, 2020, **142**, 11203–11218.

91 S. L. Apps, P. W. Miller and N. J. Long, Cobalt(-i) triphos dinitrogen complexes: activation and silyl-functionalisation of N₂, *Chem. Commun.*, 2019, **55**, 6579–6582.

92 T. D. Lohrey, R. G. Bergman and J. Arnold, Controlling dinitrogen functionalization at rhenium through alkali metal ion pairing, *Dalton Trans.*, 2019, **48**, 17936–17944.

93 T. R. Dugan, K. C. MacLeod, W. W. Brennessel and P. L. Holland, Cobalt–Magnesium and Iron–Magnesium Complexes with Weakened Dinitrogen Bridges, *Eur. J. Inorg. Chem.*, 2013, **2013**, 3891–3897.

94 T. A. Betley and J. C. Peters, Dinitrogen Chemistry from Trigonally Coordinated Iron and Cobalt Platforms, *J. Am. Chem. Soc.*, 2003, **125**, 10782–10783.

95 G. E. Greco and R. R. Schrock, Synthesis, Structure, and Electrochemical Studies of Molybdenum and Tungsten Dinitrogen, Diazenido, and Hydrazido Complexes That Contain Aryl-Substituted Triamidoamine Ligands, *Inorg. Chem.*, 2001, **40**, 3861–3878.

96 M. B. O'Donoghue, W. M. Davis, R. R. Schrock and W. M. Reiff, Heterobimetallic Dinitrogen Complexes That Contain the $\{[N_3N]Mo-NN\}^-$ Ligand, *Inorg. Chem.*, 1999, **38**, 243–252.

97 M. B. O'Donoghue, W. M. Davis and R. R. Schrock, Derivatization of Dinitrogen by Molybdenum in Triamidoamine Complexes, *Inorg. Chem.*, 1998, **37**, 5149–5158.

98 H. F. Klein, H. Koenig, S. Koppert, K. Ellrich and J. Riede, Cobalt diazenides of Main Group 1–3 metals: X-ray structure of a Grignard compound containing (dinitrogen)(trimethylphosphine)cobaltate anions, *Organometallics*, 1987, **6**, 1341–1345.

99 N. Jori, J. J. Moreno, R. A. K. Shivaraam, T. Rajeshkumar, R. Scopelliti, L. Maron, J. Campos and M. Mazzanti, Iron promoted end-on dinitrogen-bridging in heterobimetallic complexes of uranium and lanthanides, *Chem. Sci.*, 2024, **15**, 6842–6852.

